Bestrophin-4 relays Hes4 and interacts with Twist1 to suppress epithelial-to-mesenchymal transition in colorectal cancer cells

Zijing Wang[1], Bihan Xia[1], Shaochong Qi[1], Xian Zhang[1], Xiaoshuang Zhang[1], Yan Li[1], Huimin Wang[1], Miao Zhang[2,3], Ziyi Zhao[4], David Kerr[2], Li Yang[1], Shijie Cai[2*] and Jinlin Yang[1*]

1. Department of Gastroenterology and Hepatology, Sichuan University-University of Oxford Huaxi Joint Centre for Gastrointestinal Cancer, West China Hospital, Sichuan University, Chengdu 610000, China

2. Nuffield Division of Clinical Laboratory Sciences, Radcliffe Department of Medicine, University of Oxford, John Radcliffe Hospital, Oxford OX3 9DU, UK

3. College of Acupuncture and Moxibustion, Fujian University of Traditional Chinese Medicine, Fuzhou, 350102, China.

4. TCM Regulating Metabolic Diseases Key Laboratory of Sichuan Province, Hospital of Chengdu University of Traditional Chinese Medicine, Chengdu, 410000, China

***Correspondence:** yangjinlin@wchscu.cn, shijie.cai@ndcls.ox.ac.uk

*Prof. Jinlin Yang

Sichuan University-University of Oxford Huaxi Joint Centre for Gastrointestinal Cancer，Department

of Gastroenterology and Hepatology, West China Hospital, Sichuan University

Chengdu 610000, China

Tel: +86-18980602058

Fax: +86-28-85423387

Email: yangjinlin@wchscu.cn

*Dr. Shijie Cai

Nuffield Division of Clinical Laboratory Sciences, Radcliffe Department of Medicine

University of Oxford, John Radcliffe Hospital

Oxford OX3 9DU, UK

Tel: +44-1865-221110

Fax: +44-1865-220980

Email: shijie.cai@ndcls.ox.ac.uk

Running Title: BEST4 deters EMT by downregulating Twist1 expression

Abstract: Bestrophin isoform 4 (*BEST4*) is a newly identified subtype of the calcium-activated chloride channel family. Analysis of colonic epithelial cell diversity by single cell RNA-sequencing has revealed the existence of a cluster of *BEST4*+ mature colonocytes in humans. However, if the role of *BEST4* is involved in regulating tumour progression remains largely unknown. In this study, we demonstrate that *BEST4* overexpression attenuates cell proliferation, colony formation, and mobility in colorectal cancer (CRC) *in vitro*, and impedes the tumor growth and the liver metastasis *in vivo*. *BEST4* is coexpressed with hairy/enhancer of split 4 (*Hes4*) in the nucleus of cells, and *Hes4* signals *BEST4* by interacting with the upstream region of the *BEST4* promoter. *BEST4* is epistatic to *Hes4* and downregulates Twist1, thereby inhibiting epithelial-to-mesenchymal transition (EMT) in CRC. Conversely, knockout of BEST4 using CRISPR/Cas9 in CRC cells revitalises tumor growth and induces EMT. Furthermore, the low level of the *BEST4* mRNA is correlated with advanced and the worse prognosis, suggesting its potential role in regulating CRC progression.

Keywords: Colorectal cancer; Bestrophin 4; Hairy/enhancer of split 4; Twist1; Epithelial-mesenchymal transition;

Introduction

Colorectal cancer (CRC) is a common tumour worldwide. A steady increase in the morbidity and mortality of CRC has been reported (Rawla et al., 2019). When diagnosed in advanced stages, epithelial-mesenchymal transition (EMT) may occur as CRC metastasize to distal organs (Pastushenko and Blanpain, 2019; Sunlin Yong, 2021; Yeung and Yang, 2017; Zhang et al., 2021). EMT is a reprogramming process in which epithelial E-cadherin and ZO-1 are suppressed, and mesenchymal N-cadherin and vimentin are induced, transcriptionally mediated by Twist and the Snail family (Dongre and Weinberg, 2019). Overexpression of Twist1 significantly enhances the migration and invasion capabilities of colorectal cancer cells; furthermore, it is closely associated with metastasis and poor prognosis in patients with colorectal cancer (Yusup et al., 2017; Zhu et al., 2015).

The inhibition of EMT in breast cancer and prostate cancer has been associated with calcium-activated chloride channels (CaCCs) (Porretti et al., 2018; Walia et al., 2012), leading to various evaluations of CaCCs as a potential for cancer therapy (Li et al., 2017; Miotto and Struhl, 2006; Qu et al., 2019; Sui et al., 2014). The bestrophin (*BEST*) chloride channel, which is a member of a recently identified gene family, encodes several integral membrane proteins expressed on the basolateral membranes of epithelial cells; they regulate CaCCs to maintain homeostasis (Marmorstein et al., 2009; Tsunenari et al., 2003). Although there are four human evolutionarily-related genes

(*BEST1–BEST4*) (Miller et al., 2019; Tsunenari *et al*., 2003), *BEST4* is expressed predominantly in the colon (Fagerberg et al., 2014), where it gates electrolyte transportation in human intestinal epithelial cells (Ito et al., 2013). However, its role and the mechanism in regulating the development of CRC are currently unknown.

In a recent analysis based on single cell RNA-sequencing analysis, it was discovered that a group of mature colonocytes expresses *BEST4* (Parikh et al., 2019), and the subset of this group coexists with hairy/enhancer of split 4 positive (*Hes4*$^{+}$) cells (Parikh *et al*., 2019). *Hes4* belongs to a family of seven Hes genes (*Hes1–7*) that encodes a transcription factor with a basic helix-loop-helix motif. It is known to play a critical role in determining the fate and differentiation of progenitor cells during the development of various organs. The previous study has demonstrated the antagonistic role of Hes4 in regulating Twist1 through protein-protein interaction, which governs the differentiation of bone marrow stromal/stem cell lineage ((Cakouros et al., 2015). Inhibiting the Twist1 transcriptional factor has been shown to mediate commitment to the differentiation of human bone marrow stem cells, as reported by several studies (Cakouros *et al*., 2015; El Yakoubi et al., 2012; Murato and Hashimoto, 2009; Nichane et al., 2008). Given this information, it is tempting to speculate that BEST4 may be associated with Hes4 and Twist1 in regulating EMT during CRC progression.

The objectives of the present study are as follows: (1) to establish the role of BEST4 in CRC growth both in vitro and in vivo; (2) to determine the underlying molecular mechanisms by which BEST4 interacts with Hes4 and Twist1, thereby inducing EMT; and (3) to investigate the correlation between BEST4 expression and prognosis of CRC.

Results

BEST4 inhibits CRC proliferation, clonogenesis, migration, and invasion *in vitro*

To evaluate the effect of BEST4 on tumour growth, we constructed *BEST4*-expressing HCT116 and Caco2 CRC cell lines (**Figure 1-figure supplement 1A-1C)** and showed that *BEST4* overexpression halved cell proliferating rates of their respective empty vector (EV) controls when they were monitored in live and analysed using InCucyte (**Figures 1A and 1B**). This was accompanied by decreased cell viability (**Figure 1-figure supplement 1D and 1E)**. To determine the causal role of BEST4 in CRC tumorigenesis, we knocked out the *BEST4* in HCT-15 using a CRISPR/Cas9 system (**Figure 1-figure supplement 1F-H**). Consequently, there was a 50% increase in proliferation rates and viability compared with the parental control (**Figures 1C and 1D; Figure 1-figure supplement 1I**). Rescued expression of BEST4 was able to reverse the observed effects on HCT-15 (**Figure 1D; Figure 1-figure supplement 1I**).

In contrast to the controls, BEST4 overexpression decreased colony formations of HCT116 and Caco2 by 60% and 70%, respectively (**Figure 1E**). While BEST4 deletion increased the number of colonies by five-fold in HCT-15 (**Figure 1F**), the rescued expression counteracted its enhancement (**Figure 1F**).

Furthermore, overexpression of *BEST4* in HCT116 inhibited transwell migration and invasion by 70% and 80%, respectively, compared to EV controls (**Figure 1G**). But *BEST4* ablation in HCT-15

increased cell migration and invasion by two-fold and three-fold, respectively. These pro-tumor effects on HCT-15 were also reversible when BEST4 expression was rescued (**Figure 1H**).

Collectively, these findings suggest the functional inhibitory effects of BEST4 on CRC development *in vitro*.

BEST4* deters EMT in CRC *in vitro* and *in vivo

Because EMT initiation is a critical process in tumour progression (Acloque et al., 2009), we evaluated the effect of *BEST4* on EMT using qPCR and found that *BEST4* expression upregulated *CDH1* and *ZO-1* and downregulated *vimentin* and *Twist1* in HCT116 compared with the control ($p < 0.05$) (**Figures 2A**). Conversely, knockout of *BEST4* in HCT15 downregulated *CDH1* and *ZO-1* and upregulated *vimentin* and *Twist1*. Rescued expression of BEST4 in HCT-15 reversed these gene alterations (**Figures 2B**). Changes of these genes were consistent with their corresponding protein expression as analysed by immunoblotting (**Figures 2C and 2D; Figure 2-figure supplement 1A-1C**).

Next, we subcutaneously implanted *BEST4*-HA-expressing HCT116 and EV control cell lines into BALB/c nude mice and monitored tumour growth weekly. When they reached the maximum allowable volumes (day 32), the animals were culled, and tumours were harvested. Essentially, the sizes and weights of tumours in *BEST4* overexpression group were only half of the EV control (**Figures 2E and 2F**), in conjunction with the similar magnitude reduction of Ki67+ cells as analyzed by immunohistochemistry (**Figure 2G and 2H**). Further analysis of the HCT116 tumour tissue lysates

showed that *BEST4* deterred EMT by upregulating E-cadherin and, downregulating vimentin and Twist1 (**Figures 2I; Figure 2-figure supplement 1D**).

We also evaluated the inhibitory role of BEST4 in a model of CRC to the liver metastasis by intrasplenically injecting HCT-15 cell lines with BEST4 knockout (BEST4gRNA) or the wild-type control (gRNA) or the knockout with the rescue (BEST4-Rescued) into BALB/c nude mice. We observed that there were 2-fold greater of the liver metastatic nodules in the BEST4 deficient tumors than the control (**Fig. 2J-L**). Conversely, the reconstituted BEST4 expression had no visible metastatic nodules in the liver, and the pathological analysis of the tissue sections by H&E staining also confirmed no detectable metastatic loci in the tissue sections (**Fig. 2J-L**).

These findings indicate the role of BEST4 in suppressing CRCgrowth, through counteracting EMT induction in models of *in vitro* and *in vivo*.

Hes4 upstream regulation of BEST4

Given the co-expression of *BEST4*$^+$ and *Hes4*$^+$ in a human colonic epithelial lineage (Parikh *et al.*, 2019), we sought to investigate their biological interactions during tumour growth. The human CRC cell line, HCT116, was chosen for *Hes4* overexpression due to its relatively lower expression of *Hes4* compared to other CRC cell lines. Similarly, the LS174T cell line derived from human CRC was selected for *Hes4* knockdown because it exhibited comparatively higher expression of *Hes4* in comparison to other CRC cell lines **(Figure 3-figure supplement 1A)**. Upon transfecting the Flag-*Hes4* plasmid DNA into HCT116, we observed a responsive upregulation of both endogenous *BEST4* mRNA and protein levels compared to the control transfectant (**Figure 3A; Figure 3-figure**

supplement 1B and 1C). This intrinsic association was further supported by knocking down the endogenous Hes4 with two pairs of shRNAs in LST174 that resulted in downregulation of endogenous BEST4 (**Figure 3B; Figure 3-figure supplement 1D and 1E**).

To explore how Hes4 regulates *BEST4* expression at the transcriptional level, we transfected a *BEST4* promoter-driven luciferase DNA construct into *Hes4*-expressing HCT116 and assessed the promoter activity using a dual-luciferase assay. Our results showed a four-fold increase in the promoter activity compared to the EV control (**Figure 3C**), Furthermore, ChIP-qPCR analysis using a Flag antibody to IP for Hes4 revealed a twelve-fold enrichment of the P3 region upstream of the *BEST4* transcriptional start site compared to the control (**Figure 3D**). Interestingly, *BEST4* overexpression in HCT116 cells did not affect *Hes4* mRNA expression as quantified by qPCR (**Figure 3-figure supplement 1F**), suggesting that *Hes4* regulates *BEST4* expression upstream. This speculation is supported by immunofluorescence staining, where we observed nuclear co-localization of BEST4 (green) and Hes4 (red) in HCT116 cells co-transfected with *BEST4*-HA and Flag-*Hes4* plasmid DNAs, along with additional cytoplasmic expression of *BEST4* (**Figure 3E)**.

To evaluate the association of *BEST4* with Hes4 at the translational level, we co-transfected their HA-tagged *BEST4* and Flag-*Hes4* plasmid DNAs into HEK293 cells, along with the respective single transfectant control. By conducting IP with antibodies specific to Flag or HA, we showed that *BEST4* and *Hes4* were reciprocally copurified from the nuclear protein lysates, but not with IgG controls (**Figure 3F**).

Collectively, these findings indicate that *BEST4* interacts with *Hes4* at both transcriptional and

translational levels.

BEST4 relays _Hes4_ signal and downregulates Twist1 leading to EMT inhibition independent of the channel function in CRC

Because a step of *Hes4* in committing to human bone marrow stromal/stem cell lineage-specific development is mediated by Twist1 downregulation (Cakouros *et al.*, 2015), with evidence of direct interaction between BEST4 and Hes4 observed in HCT116, it is plausible that they could exploit Twist1 to regulate EMT. To test this notion, we transfected a Twist1 promoter-driven luciferase DNA construct into HCT116. In comparison with the EV control, Flag-*Hes4* or *BEST4*-HA transfectants significantly decreased Twist1 promoter activity by almost half, as evaluated by the dual-luciferase assay (**Figure 4A)**. Essentially, the *BEST4* transfectant enhanced inhibition of the Twist promoter by 70% in *Hes4*-expressing HCT116 **(Figure 4B; Figure 4-figure supplement 1A),** hence suggesting that *BEST4* mediates the inhibition of the Twist1 promoter activity by *Hes4*. This effect was also observed when endogenous Hes4 was knocked down using shRNAs in HCT116 cells transfected with *BEST4*-HA plasmid DNA (**Figure 4C**).

The association of BEST4 with the Twist1 promoter activity was also evidenced by their nuclear colocalization after transfecting BEST4-HA and Myc-Twist1 plasmid DNAs into HCT116 (**Figure 4-figure supplement 1B)**. Co-IP with antibodies to Myc or HA showed that they were copurified from the nuclear protein lysates, but not with the IgG controls from the transfectant cell lysates (**Figure 4D**；**Figure 4-figure supplement 1B**). Additionally, the knockdown of endogenous *BEST4* in Hes4-expressing HCT116 cells substantially decreased Flag-Hes4 coprecipitation from the nuclear

protein lysates, while Myc-Twist1 expression remained constant, as determined by co-IP with antibodies to Flag or My (**Figure 4E；Figure 4-figure supplement 1C**).

We then investigated the impact of Hes4 expression on EMT induction by overexpressing Hes4 in HCT116 cells. Our results showed there were upregulation of ZO-1 and E-cadherin epithelial molecules, and downregulation of Twist1 protein (**Figure 4F; Figure 4-figure supplement 2A)** and the *vimentin* mRNA **(Figure 4-figure supplement 1D)**. The vimentin protein appeared to be undetectable in HCT116, which was consistent with a previous report (Roger et al., 2010). Nevertheless**,** knocking down endogenous *Hes4* in LS174T cells using shRNAs targeting two *Hes4* domains caused the opposite effect **(Figure 4G; Figure 4-figure supplement 2B).**

To determine if BEST4 is downstream signal that relays Hes4 to regulate Twist1 expression and consequently EMT induction, we knocked down endogenous *BEST4* with siRNAs in Hes4-expressing HCT116 and showed the corresponding downregulation of E-cadherin and ZO-1, with upregulation of Twist1 protein and the *vimentin* mRNA, as analyzed by immunoblotting and qPCR **(Figure 4H; Figure 4-figure supplement 2C; Figure 4-figure supplement 1ED**). The opposite was true when BEST4 was overexpressed in LS174T **(Figure 4I; Figure 4-figure supplement 2D**). *Hes4*Hence, inhibition of EMT induction by Hes4 is BEST4-mediated by downregulation of Twist1 expression in CRC

Given the physiological role of *BEST4* plays in regulating chloride/calcium flux, we evaluated the channel functional effect on EMT induction. After respectively incubating *BEST4*-expresing HCT116 and the EV control with 300μM DIDS (a broad blocker of chloride channel), or a gradient increase in

doses of CaCCinh-A01 (a specific inhibitor of native calcium-activated chloride channels), or 1μM ionomycin (a calcium ionophore to activate the chloride channel) as published previously (Liu *et al*, 2015; Uwada *et al*, 2019), we showed that *BEST4* significantly increased chloride/calcium fluxes and activated their exchanges and the expected inhibition by DIDS, CaCCinh-A01 or ionomycin (**Figure 5-figure supplement 1A-1C**). Through immunoblotting analysis, we recapitulated that *BEST4* simultaneously upregulated both ZO-1 and E-cadherin, and downregulated Twist1. Essentially, the levels of these proteins remained constantly expressed when the cells were treated with DIDS or CaCCinh-A01 or ionomycin, respectively (**Figure 5-figure supplement 1D-1F**). Hence, these results suggest *BEST4* protein-mediated EMT suppression is independent of its channel function in HCT116.

Correlation of the *BEST4* with clinicopathology and outcomes of patients diagnosed with CRC

We showed evidence of the endogenous *BEST4* mRNA and protein expression in HCT116 and LS174T CRC cell lines (**Figures 3A and 3B**); these findings prompted us to explore the potential clinically significant *BEST4* expression in CRC. Initially with high-throughput whole transcriptome sequencing analysis of five pairs of CRCs and adjacent normal tissues (ANTs), we identified several significantly downregulated genes in CRC compared to ANTs; *BEST4* was in the top four **(Figures 5A and 5B)**. Further validation by qPCR in the paired tissues of 50 colorectal adenomas and 124 CRC showed that the *BEST4* was expressed significantly less in adenomas and tumours than in ANTs **(Figures 5C and 5D**). Immunoblotting analysis of tissue lysates from five paired randomly selected samples showed that BEST4 protein was downregulated in CRC (**Figures 5E; Figure 5-figure supplement 1G**). Using public datasets of The Cancer Genome Atlas (TCGA) and the

Genotype-Tissue Expression (GTEx), we measured *BEST4* mRNA expression in CRC and matched normal tissues with the online Gene Expression Profiling Interactive Analysis (GEPIA) tool (http://gepia.cancer-pku.cn/). As shown in **Figure 6-figure supplement 1A,** the normal colorectal control tissues consistently expressed higher *BEST4* than the CRC.

We further evaluated the clinicopathological significance of *BEST4* expression in CRC patients by examining its correlation with gender, tumour-node-metastases stage, and lymph node metastasis based on the eighth edition of the American Joint Committee on Cancer Staging Manual (M. B. Amin et al., Springer, 2017). Interestingly, low *BEST4* mRNA expression in males was twice as high as in females (p=0.022, **Table 1**). Accordingly, low *BEST4* mRNA expression correlated with more advanced stages (p=0.02, **Table 1**) and lymph node metastasis (between 0 and 2) (p=0.032, **Table 1**). Patients with high *BEST4* expression had better overall survival than those with low expression (p<0.01, **Figure 5F**), which was confirmed by univariate survival analysis showing a lower risk of death (p<0.001, **Table 2**). Multivariate Cox regression analysis indicated that low levels of BEST4 mRNA were associated with poor prognosis of CRC patients (Hazard Ratio [HR], 0.285; 95% confidence interval, 0.157–0.606; P<0.001; **Table 2**).

After the significant reduction of the *Hes4* mRNA expression through RNA sequencing analysis of our CRC patients (**Figure 6-figure supplement 1B and 1C**), we proceeded to investigate the connection between *BEST4* and *Hes4* in TCGA and GTEx (http://gepia.cancer-pku.cn/). Our findings revealed a positive correlation between these genes (R = 0.47, p<0.001) (**Figure 6-figure supplement 1D**), providing further evidence of their association in CRC. Furthermore, we conducted additional

mining of TCGA or GTEx datasets using the GEPIA tool (http://gepia.cancer-pku.cn/) and observed a positive correlation between *BEST4* and the *CDH1* mRNA (R = 0.77, $p<0.001$), with a negative correlation with *vimentin* (R =–0.49, $p<0.001$) and *Twist* mRNA (R =–0.39, $p<0.001$)) (**Figure 6-figure supplement 1E-G**). These correlation analyses of RNA sequencing data from our patients and publicly available datasets underscore the association of low *BEST4* expression with worse outcomes in malignant CRC.

Discussion

In cancer cell cultures and mouse tumour xenografts, the present study shows that *BEST4* inhibits the development of CRC. An axis comprising *Hes4/BEST4/*Twist1 governs the induction of EMT in CRC. *BEST4* interacts with *Hes4* at the transcriptional and translational levels, and downregulates Twist1 expression, resulting in EMT inhibition but independent of its channel functions. Our findings support the notion in several ways: (1) *Hes4* binds to the promoter region of *BEST4*; (2) *BEST4* colocalizes with *Hes4* and Twist1 in the nucleus of cells, and protein-protein interactions; (3) the *BEST4* inhibitory role in EMT exhibits upregulation of epithelial ZO-1 and E-cadherin, and downregulation of mesenchymal vimentin and Twist1 in CRC; and finally (4) low *BEST4* mRNA levels were significantly correlated with malignant lesions and worse outcomes of CRC patients. To the best of our knowledge, this is the first characterization of the role of *BEST4* in suppressing CRC progression and the underlying molecular mechanisms.

CaCCs are expressed widely in several types of epithelial and endothelial cells and are classified as calcium-dependent chloride channels (e.g., anoctamin-1 [ANO1 or TMEM16]), chloride channel accessory proteins (CLCAs), and members of the BEST family. The latter is a recent addition to the class of molecularly defined chloride channels (Huang et al., 2012). Calcium-dependent chloride channels and CLCAs are differentially expressed in CRC and normal colon tissues, exerting pro- or anti-growth effects, while little is known of BEST family in CRC (Li *et al.*, 2017; Sanders et al., 2012; Sui *et al.*, 2014; Yang et al., 2015). There are four subtypes of the *BEST* family in mammals that assemble as pentamers to form Ca^{2+}-activated Cl^- channels and maintain cellular physiological functions (Marmorstein *et al.*, 2009; Milenkovic et al., 2008; Tsunenari *et al.*, 2003). Subtypes of *BEST1-3* are responsible for vitelliform macular dystrophy, regulating the cilia of olfactory sensory neuronal activity; others regulate cGMP-dependent calcium-activated chloride conductance in vascular smooth muscle cells (Matchkov et al., 2008; Pifferi et al., 2009). An intrinsic function of the *BEST4* gene in modulating CRC growth remains poorly illustrated. In the present study, we demonstrated that *BEST4* functionally inhibits the development of CRC *in vitro* and *in vivo*. *BEST4* is transcriptionally regulated and physically interacts with upstream *Hes4*, leading to downregulation of Twist1 and EMT suppression. This suppression is independent of physiological Ca^{2+}-activated Cl^- channels since inhibition of BEST4-associated Ca^{2+}-and Cl^- fluxes did not alter ZO-1/E-Cadherin and Twist1 protein expression.

The recent identification of a heterogeneous *BEST4*$^+$ and *Hes4*$^+$ subgroup in a human colonic epithelial lineage (Parikh *et al.*, 2019) led us to consider their potential role in regulating CRC progression. Among the Hes family, which is associated with intestinal progenitor cells in adenoma

transformation, *Hes1* and *Hes4* are a paralog pair, with other members more distantly related (Katoh and Katoh, 2004). While *Hes1* has been reported to induce EMT and promote metastasis and chemoresistance in CRC (Sun et al., 2017; van Es et al., 2005; Yuan et al., 2015), *Hes4* is identified by our present study capable of combating EMT induction in a *BEST4*-dependent manner that is regulated at both transcriptional and translational levels.

The process of EMT transforms epithelial cells exhibiting a spindle fibroblast-like morphology, leading to the acquisition of mesenchymal characteristics and morphology, enabling these cells to acquire invasive and migratory abilities, with expression switching epithelial E-cadherin and Zo-1 to mesenchymal vimentin (Dongre and Weinberg, 2019). When diagnosed in advanced stages, EMT may occur as CRC metastasize to distal organs (Pastushenko and Blanpain, 2019; Sunlin Yong, 2021; Yeung and Yang, 2017; Zhang et al., 2021).The whole process is regulated by transcriptional factors of the Snail family and Twist1(Dongre and Weinberg, 2019). Twist1 (a **basic helix-loop-helix** transcription factor) reprograms EMT by repressing the expression of E-cadherin and ZO-1 (Nagai et al., 2016; Yang et al., 2004) and simultaneously inducing several mesenchymal markers, typically vimentin (Bulzico et al., 2019; Meng et al., 2018; Nagai *et al.*, 2016; Yang *et al.*, 2004), which is a pivotal predictor of CRC progression (Vesuna et al., 2008; Yang *et al.*, 2004; Yusup et al., 2017; Zhu et al., 2015). The Twist1 transcriptional factor plays a crucial role in inducing EMT, which contributes to the malignant lesions (Yang et al., 2004). Its physical interaction with *Hes4* determines human bone marrow stromal/stem cell differentiation (Cakouros *et al.*, 2015). Twist1, a basic helix-loop-helix transcription factor, represses the expression of E-cadherin and ZO-1 and induces several mesenchymal markers including vimentin, which is a pivotal predictor of CRC

progression (Nagai et al., 2016; Yang *et al.*, 2004) (Bulzico et al., 2019; Meng et al., 2018; Nagai *et al.*, 2016; Vesuna et al., 2008; Yang *et al.*, 2004; Yusup *et al.*, 2017; Zhu *et al.*, 2015). Overexpression of Twist1 significantly enhances the migration and invasion capabilities of colorectal cancer cells; furthermore, it is closely associated with metastasis and poor prognosis in patients with colorectal cancer(Yusup *et al.*, 2017; Zhu *et al.*, 2015). Despite Twist1 importance in CRC, little is known about how it is controlled during EMT induction. Our present study reveals that Twist1 colocalized and interacted with *BEST4* in the nucleus of CRC HCT116 cells, leading to downregulation of Twist1 and inhibition of EMT. *Hes4* also caused the same effect, but through intermediation with *BEST4*. Although the mechanistic insights of their interplay remain to be elucidated, the present study identifies the *Hes4-BEST4-Twist1* axis that contributes to counter EMT in the development of CRC **(Figure 5G)**.

Lastly, our analysis of correlations reveals the clinical significance of *BEST4* expression in CRC. In particular, the mRNA levels of *BEST4* were lower in tissues of both precancerous adenomatous lesions and CRC than ANTs. These alterations are significantly correlated with large tumour size, positive nodes, and poor overall survival, especially in male patients. Interestingly, a previous study conducted on a Chinese cohort reported an approximately 40% higher incidence of CRC in males than in females (Zhang et al., 2019). But it remains to be investigated whether sex hormone-related factors plays a role in the gender-specific downregulation of *BEST4* and its impact on CRC in males (Yu et al., 2020).

In conclusion, the functional significance of *BEST4* in CRC development and its interplay with other molecules is completely unknown. The present study demonstrates the role of *BEST4* in

inhibiting CRC proliferation, migration, and invasion both in models of in vitro and in vivo. Mechanically, *BEST4* is epistatic to *Hes4* for downregulating Twist1 and inhibits EMT in CRC. Therefore, we reveals a previously unknown mechanism of the *Hes4-BEST4-Twist* axis that restrains the progression of CRC.

Materials and Method

Clinical samples

A total of 124 samples of paired CRC and adjacent normal tissue and 50 samples of paired adenoma and ANT were collected randomly from clinical specimens from patients undergoing intestinal resections or upper gastrointestinal endoscopies at the Department of Gastrointestinal Surgery and Digestive Endoscopy Centre, West China Hospital, China, between January and December 2013. All patients were followed until December 2018 or until death. Samples from patients with malignant tumours in other organs, from patients who received preoperative chemotherapy or radiotherapy, and from patients with incomplete follow-up data were excluded. The survival time was calculated from the surgery date to the follow-up deadline (above) or until the date of death. The Ethics Committee of West China Hospital, Sichuan University (Sichuan, China) approved the study. All procedures were performed per the 1964 Declaration of Helsinki. Written informed consent was obtained from all participants.

Cell cultures and reagents

The human colon cancer cell lines Caco-2, HCT116, HCT-15, and LS174T were purchased from The American Type Culture Collection (Manassas, VA, USA). Cells were authenticated using short tandem repeat analysis performed within two years of receipt. Cells at passages >15 were not used. All cells were maintained in Dulbecco's Modified Eagle's medium (DMEM; Gibco, Waltham, MA, USA) supplemented with 10% foetal bovine serum (FBS), 100 U/mL penicillin, and 100 mg/mL streptomycin. Before each experiment, cells were provided with low glucose (1 g/L) DMEM with 5% FBS before adding experimental reagents. All cell lines were frequently examined using the MycoAlert™ Mycoplasma Detection Kit (Lonza, Verviers, Belgium) to ensure they remained free of mycoplasma contamination.

Tumour and CRC hepatic metastasis mouse xenografts

Four-week-old female BALB/c nude mice were housed under standard conditions. The mice were randomized into two groups, with eight mice per group. HCT116 cells (5×10^6 cells in 0.1 mL phosphate-buffered saline) transduced with the lentivirus containing *BEST4* or EV were injected subcutaneously into the right dorsal flank of mice. Tumour growth was measured twice a week using callipers, and tumour volumes were calculated as length x width^2 x 0.5. Mice were sacrificed at 32 days, and tumour weight was measured at the end of the experiment. For further analysis, the excised tumour tissues were divided into two parts and embedded in paraffin or preserved at −80 °C for further analysis.

For the liver metastasis of CRC, intrasplenic injections of HCT-15 cells with BEST4-knockout (BEST4-gRNA), BEST4-rescued or control (EV-gRNA) (5×10^6 cells in 0.1 mL PBS) were performed

into 6-week-old Balb/c nude mice as described previously[2]. There were 3 mice/group. Briefly, at day 28 after the procedure, mouse livers were paraffin embedded and the sections for H&E staining. The numbers of the metastatic nodules on the livers were double-blind visually quantified and confirmed by a pathologist.

The Animal Ethics Committee approved animal experiments of West China Hospital, Sichuan University (Sichuan, China).

CRC cell lines with overexpression of *BEST4*

Forced overexpression of *BEST4* was examined in HCT116 and Caco2 CRC cells in which the C-terminal HA epitope-tagged human *BEST4* gene with GFP (*BEST4*-HA-GFP) or GFP alone was introduced by lentivirus-mediated gene transfer. Fluorescence-activated cell sorting (FACS) was performed to obtain single cells distributed into 96-well plates. Three independent lines with the highest levels of BEST4 expression were used for subsequent experiments (**Figures S1A and S1B**). *BEST4* mRNA and HA-tagged protein levels were significantly higher in HCT116 and Caco2 cells transfected with *BEST4*-HA plasmids than those transfected with the empty vector (EV) alone (**Figure S1C**). The *BEST4*-overexpressing cell lines were named "HCT116 *BEST4*-HA" and "Caco2 *BEST4*-HA." Cells transfected with the EV alone were referred to as "HCT116 EV" and "Caco2 EV."

CRISPR/Cas9-mediated knockout of *BEST4*

BEST4-depleted HCT-15 cells were generated with CRISPR/Cas9 gene-editing technology using a dual sgRNA approach. Two sequences that targeted exon 3 within the *BEST4* active fragment

(5'-TGACTCTCGTGGTGAACCGC-3' and 5'-CCGAGATGACGCACATCAGC -3') were inserted into the pU6-gRNA-Cas9-EGFP vector (GenePharma, Shanghai, China) to generate a CRISPR/Cas9 *BEST4* knockout plasmid. Excision of the targeted 44 bp genomic fragment resulted in splicing errors in exons 2 to 4 and generated a premature STOP codon that abrogated functional gene expression (**Figures S1F and S1G**). Cells were transfected with these plasmids, and GFP^+ cells were FACS-sorted as single cells into 96-well plates. After culturing for three weeks, cells were distributed into two 24-well plates, and the appropriate deletion was verified by sequencing. Only cell lines with homozygous deletions were used. Three independent lines generated using this method were used for subsequent experiments and were named "HCT15 *BEST4*-gRNA." Diminished expression of immunoreactive BEST4 protein was confirmed by immunoblotting (**Figure S1H**). The same overexpression strategy was adopted to rescue BEST4 expression in *BEST4* knockout HCT-15 cells, named "HCT15 *BEST4*-Rescued."

Plasmids and transfection/transduction

Expression plasmids encoding *BEST4* (GeneID: 266675, NM_153274; vector: pCDH-CMV-MCS-EF1-CopGFP-T2A-Puro) containing a C-terminal hemagglutinin (HA) epitope tag, *HES4* (GeneID: 57801, NM_001142467.2; vector: pCDH-CMV-MCS-EF1- CopGFP-T2A-Puro) containing a N-terminal Flag epitope tag,were synthesized by Public Protein/Plasmid Library (Nanjing, China). According to the manufacturer's instructions, Lipofectamine 3000 (Invitrogen, Carlsbad, CA, USA) was used in cell transfection experiments.

To generate a model of CRC with forced overexpression of *Hes4*, cells were transfected with lentiviral pCDH-CMV-MCS-EF1-CopGFP-T2A-Puro vectors containing human Hes4 cDNA and selected with puromycin (Invivogen, San Diego, CA, USA) at 10 μg/mL introduced 48 h after transfection.

For short hairpin RNA (shRNA) and RNA silencing (siRNA) experiments, HEK293 cells were co-transduced with lentiviral vectors carrying shRNA targeting *HES4* (Public Protein/Plasmid Library, Nanjing, China; target sequences are listed in **Table S1**). Supernatants were collected at 48 and 72 h for analysis. Scrambled shRNAs were used to control for non-specific effects. Transduction was performed by mixing aliquots of lentivirus with a standard medium containing 10 μg/mL puromycin (Invivogen) to remove untransduced cells. GeneSolution siRNAs targeting *BEST4* (*BEST4*-siRNA) were used to silence gene expression. Scrambled siRNA (SCR) was used as a control (Qiagen, Hilden, Germany). The target sequences of the *BEST4* siRNAs are listed in **Table S1**. For siRNA experiments, cells were seeded one day before transfection in an antibiotic-free medium and grown to 60% confluency in six-well plates. Cells were transfected using Lipofectamine 3000 as per the manufacturer's protocol. The efficiency of RNA interference was determined using quantitative polymerase chain reaction (qPCR) and western blotting.

RNA isolation, cDNA library preparation, sequencing, and data analysis

Total RNA was isolated using a High Pure RNA Isolation Kit (Roche, Basel, Switzerland). RNA samples with an RNA integrity number (RIN) ≥7.0 and a 28S:18S ratio ≥ 1.5 were used in subsequent experiments. Sequencing libraries were generated and sequenced by CapitalBio Technology (Beijing,

China). A total amount of 3 μg RNA per sample was used. Briefly, the Ribo-Zero™ Magnetic Kit (Epicentre) was used to remove rRNA from the total RNA, and then the NEBNext Ultra RNA Library Prep Kit for Illumina (NEB, USA) was used to construct the libraries for sequencing following the manufacturer's instructions. The RNA was fragmented into pieces of ~200 base pairs in length in NEBNext First-Strand Synthesis Reaction Buffer (5X). The first-strand cDNA was synthesized from the RNA fragments using reverse transcriptase and random hexamer primers, and then the second-strand cDNA was synthesized in Second-Strand Synthesis Reaction Buffer with dUTP Mix (10x). The end of the cDNA fragment was subjected to an end-repair process that included the addition of a single "A" base followed by ligation of the adapters. Products were purified and enriched using PCR to amplify the library DNA. The final libraries were qualified using Agilent 2100 and quantified using the KAPA Library Quantification Kit (KAPA Biosystems, South Africa). Finally, the libraries were subjected to paired-end sequencing with a paired-end 150-base pair reading length on an Illumina NovaSeq sequencer (Illumina).

The sequencing quality of raw data in *fastq* format was assessed using FastQC, and then low-quality data were filtered using the Next Generation Sequencing Quality Control platform. The high-quality clean reads were then aligned to the reference genome using Tophat2 with default parameters. The genome of the human genome version of hg38 (UCSC) was used as the reference. Cufflinks and Cuffmerge software packages were used to assemble the transcripts. All subsequent comparative analyses of lncRNAs and mRNAs were based on the results of the transcripts. Transcripts corresponding to mRNAs or lncRNAs were collected from databases and treated as known lncRNAs and annotated based on information from public databases. The transcripts were treated as novel

lncRNAs when their sequence length was >200 and when they were predicted to be non-coding RNAs. Differential expression analyses were performed using the limma package and edgeR. Functional annotation and enrichment analyses were performed using KOBAS 3.0. The target genes of the mRNAs were predicted based on cis- and trans-patterns based on the location on the reference genome and sequence similarity. The raw sequence data reported in this paper were deposited in the NCBI Sequence Read Archive with accession number PRJNA690126.

RNA extraction and real-time PCR

Total RNA was isolated from cell lysates according to the manufacturer's protocol (Zymo Research, Tustin, CA). A High-Capacity cDNA Reverse Transcription Kit (Thermo Fisher Scientific, Waltham, MA) was used for first-strand cDNA synthesis with 1 μg of total RNA from each sample. The expression of genes and the GAPDH internal control was assayed by qPCR using SYBR Green (Bioline Reagents Ltd, London, UK). Primer sequences are shown in **Table S1**.

Immunoblotting

Protein extracts were prepared using RIPA lysis buffer (Merck Millipore, Temecula, CA) containing protease inhibitor cocktail and phosphatase inhibitor tablets (Sigma, MO, USA). Protein content was determined using a protein assay kit (Bio-Rad, Hercules, CA). Western blotting was performed as described previously (Wang et al., 2019). All primary (1:1000) and secondary antibodies (1:2000), except BEST4 (1:800; LsBio, Seattle, WA) and anti-Flag M2 (Sigma, MO, USA), were purchased from Cell Signaling Technology (Danvers, MA, USA).

Cell proliferation

Cell proliferation was monitored in real time using an *IncuCyte* ZOOM live-cell microscope incubator (Essen Bioscience, MI, USA), in which the cell confluence was calculated using *IncuCyte* software, and the cell proliferation was expressed as the percentage of confluence. According to the manufacturer's protocol, a Cell Counting Kit□8 (CCK-8, Dojindo, Tokyo, Japan) assay was used to confirm cell viability. The absorbance at 450 nm was measured using a microplate reader (BioTek, VT, USA), and growth curves were drawn according to the optical density.

Clonogenesis

A total of 3×10^3 cells per well were seeded in 6-well plates. The medium was refreshed twice a week. After 2 weeks, colonies were fixed and stained with crystal violet (0.005% in 20% methanol). The numbers of colonies were quantified using GelCount (Oxford Optronix Ltd, Oxford, UK). The assay was carried out in triplicate wells for three independent experiments.

Transwell migration and invasion

Cell migration and invasion assays were performed using Transwell assay with uncoated polycarbonate transwell inserts (Millipore, Billerica MA). Cells were digested and suspended in culture medium without FBS for the migration assay. Cell suspensions were added into the upper chamber of the Transwell insert and then placed into the 24-well plate Transwell containing medium with 10% FBS in the lower chamber. For the invasion assay, the 24-well plate with Transwell inserts was coated with 50 μg/insert of Matrigel matrix on the top of the chamber (BD Biosciences, Oxford, UK). After 48 h, cells that travelled to the lower surface of the insert were stained with crystal violet. Experiments were conducted in triplicate.**Immunohistochemistry**

Paraffin-embedded tissue blocks from formalin-fixed tumour samples were sectioned, dewaxed, and rehydrated following standard protocols. Sections were stained for human Ki67 primary antibody (1:200, Cell Signaling Technology, MA, USA), a marker of cell proliferation, and anti-mouse HRP-conjugated secondary antibody (Dako, CA, USA), and the positive cells were counted in eight randomly chosen fields. Expression of BEST4-HA in tumours was stained with anti-HA primary antibody (1:800, Cell Signaling Technology) and anti-rabbit HRP-conjugated secondary antibody (Dako).

Dual-luciferase reporter assay

The *BEST4* promoter region (−2000 to +100 bp) was cloned into pGL3-basic vectors (Promega, WI, USA) to construct the luciferase reporter plasmid (pGL3-*BEST4*). The stably high Hes4 expression cell line was constructed by infecting HCT116 cells with lentivirus, and then the recombinant plasmid pGL3- *BEST4* was co-transfected with the control plasmid pRL-TK (Promega) into HCT116 Hes4 and HCT116 EV cells. Twenty-four hours after transfection, firefly and Renilla luciferase activities were analysed using the dual-luciferase reporter assay (Promega) according to the manufacturer's instructions, and the results were normalized as relative luciferase activity (firefly luciferase/Renilla luciferase).

Chromatin immunoprecipitation-quantitative PCR (ChIP-qPCR)

ChIP-qPCR was performed as previously described (Miotto and Struhl, 2006). At room temperature, we crosslinked cells at 5×10^7 cells/mL for 10 min using 1% formaldehyde and stopped the reaction using 125 mM glycine. After three washes with ice-cold PBS, cells were homogenized, lysed,

and sonicated to shear DNA into 200–500 bp fragments. The DNA fragments were incubated with 10 μg of antibodies against anti-Flag tag (Sigma, MO, USA) or native IgG (Cell Signaling Technology) followed by IP with 60 μl of protein A/G Magnetic Beads (MedChemExpress, New Jersey, USA) and overnight incubation at 4 °C with rotation. Immunoprecipitated DNAs were extracted from the DNA/antibody/protein A/G bead complexes using proteinase K digestion, subjected to reverse crosslinking at 65 °C for 4 h, and purified with spin columns. qPCR analysis was performed to determine the enrichment of DNA fragments using the indicated primers (**Table S1**). ChIP-qPCR data were normalized using the fold-enrichment method (ChIP signals were divided by IgG signals), and DHFR 5 'UTR was used as a negative control. Each experiment included triplicate samples and the data shown represent the mean of three independent experiments.

Immunofluorescence staining

HCT116 cells transfected alone or co-transfected with expression vectors encoding C-terminal HA-tagged BEST4, and N-terminal Flag-tagged Hes4 were grown on glass coverslips, fixed for 10 min with 4% paraformaldehyde, permeabilized for 5 min with 0.2% Triton X-100, then blocked for 15 min with 3% bovine serum albumin. HA-tagged *BEST4* was stained using an anti-HA antibody (Cell Signaling Technology) followed by a TRITC-labelled secondary antibody (Abcam, Cambridge, UK). Flag-tagged Hes4 was detected using an anti-Flag antibody (Sigma, MO, USA) with an Alexa Fluor 647-labeled secondary antibody (Invitrogen Carlsbad, CA). Cells were mounted and imaged using laser-scanning confocal microscopy (*Nikon* Corporation, Tokyo, Japan).

Co-immunoprecipitation (Co-IP)

Co-IP assays were performed on nuclear extracts. According to the manufacturer's protocols, nuclear proteins of each sample were collected using Minute™ Cytoplasmic and Nuclear Fractionation Kit (Invent, MN, USA). Protein G Dynabeads (Thermo Fisher Scientific, MA, USA) following the manufacturer's instructions. Briefly, HEK293 cells were co-transfected with expression vectors encoding C-terminal HA-tagged *BEST4* and N-terminal Flag-tagged Hes4. Cells were harvested and lysed 48 h after transfection. Cell lysates (500 µg) were incubated overnight at 4 °C in a rotating wheel with 2 µg of anti-FLAG (Sigma, MO, USA) or anti-HA antibody (Cell Signaling Technology) bound to Protein G Dynabeads. Immunocomplexes were separated using a magnet, washed three times in PBS with 0.02% Tween™ 20 and eluted in elution buffer (50 mM glycine pH 2.8). After boiling in sample buffer at 70 °C for 10 min, immunocomplexes were loaded on 4–20% Tris-glycine gels (Bio-Rad, CA, USA), followed by blotting on PVDF membranes and immunoblotting using the indicated antibodies.

Chloride channel efflux

Cells were maintained in a serum free DMEM overnight prior to treatment with DIDS (4,4'-diisothiocyanatostilbene-2,2'-disulfonic acid; HY-D0086, MCE, China), $CaCC_{inh}$-A01 **(**HY-100611, MCE, China) or 1 µM ionomycin for 24h as previously published (Liu *et al*, 2015; Uwada *et al*, 2019). Chloride channel efflux was evaluated with colorimetric changes by commercially available kits (ab176767, Abcam). Briefly, 40,000 *BEST4*-expressing or *EV*-control HCT116 cells were plated per well in a 96-well plate and allowed to grow over night. Before the assay, cells were refreshed with serum-free medium and 100 µL/well of pre-warmed iodide-loading buffer was added and the plate was incubated for 2 hours at 37 □. After washing each well with HBSS three times, cells

were lysed and Iodide Sensor Blue dye (50 μL/well) and 0.5 x Iodide Sensor Enhancer (50 μL/well) were added and incubated for 1 minutes before reading at 405 nm. Data was calculated as fold-change relative to control.

Statistical analysis

The results were expressed as the mean ± standard error of the mean. The statistical significance of differences between means was assessed using Student's unpaired two-tailed *t*-tests, and the Mann-Whitney U test was performed to compare the variables in two groups using SPSS 25.0 (SPSS, Chicago, USA). The relationship between the clinicopathological parameters of CRC and the expression of *BEST4* was examined using the Kruskal-Wallis H test. The Kaplan-Meier method and log-rank tests were used to assess overall survival in relation to *BEST4* expression. Differences in cell proliferation and tumour growth rates between the two groups of mice were assessed using repeated-measures analysis of variance. Western blot intensity was assessed using ImageJ v1.53 software (ImageJ, Bethesda, MD, USA). *P*-values <0.05 indicated statistically significant differences.

Data and code availability: The raw sequence data reported in this paper have been deposited in the NCBI Sequence Read Archive (SRA) with accession number PRJNA690126.

Compliance and ethics: The author(s) declare that they have no conflict of interest. The clinical studies were approved by the Ethics Committee of West China Hospital, Sichuan University (Sichuan,

China). All procedures were performed per the 1964 Declaration of Helsinki. Written informed consent was obtained from all participants. The Animal Ethics Committee approved animal experiments of West China Hospital, Sichuan University (Sichuan, China).

Acknowledgments: We thank Xuemei Cheng, Sisi Wu, and Huifang Li from Core Facilities of West China Hospital, Sichuan University, for expert technical assistance. This work was supported by the National Natural Science Foundation of China (grant numbers: 82173253, 82103539, 82074298), Sichuan Science and Technology Program (grant numbers: 2021YFH0005, 2022YFH0003), Sichuan Province cadres health research project (grant numbers: 2023104).

References

Acloque, H., Adams, M.S., Fishwick, K., Bronner-Fraser, M., and Nieto, M.A. (2009). "Epithelial-mesenchymal transitions: the importance of changing cell state in development and disease". J Clin Invest *119*, 1438-1449. 10.1172/JCI38019.

Bulzico, D., Pires, B.R.B., PAS, D.E.F., Neto, L.V., and Abdelhay, E. (2019). "Twist1 Correlates With Epithelial-Mesenchymal Transition Markers Fibronectin and Vimentin in Adrenocortical Tumors". Anticancer research *39*, 173-175. 10.21873/anticanres.13094.

Cakouros, D., Isenmann, S., Hemming, S.E., Menicanin, D., Camp, E., Zannetinno, A.C., and Gronthos, S. (2015). "Novel basic helix-loop-helix transcription factor hes4 antagonizes the function of twist-1 to regulate lineage commitment of bone marrow stromal/stem cells". Stem Cells Dev *24*, 1297-1308. 10.1089/scd.2014.0471.

Dongre, A., and Weinberg, R.A. (2019). "New insights into the mechanisms of epithelial-mesenchymal transition and implications for cancer". Nature reviews. Molecular cell biology *20*, 69-84. 10.1038/s41580-018-0080-4.

El Yakoubi, W., Borday, C., Hamdache, J., Parain, K., Tran, H.T., Vleminckx, K., Perron, M., and Locker, M. (2012). "Hes4 controls proliferative properties of neural stem cells during retinal ontogenesis". Stem cells (Dayton, Ohio) *30*, 2784-2795. 10.1002/stem.1231.

Fagerberg, L., Hallström, B.M., Oksvold, P., Kampf, C., Djureinovic, D., Odeberg, J., Habuka, M., Tahmasebpoor, S., Danielsson, A., Edlund, K., et al. (2014). "Analysis of the human tissue-specific expression by genome-wide integration of transcriptomics and antibody-based proteomics". Mol Cell Proteomics *13*, 397-406. 10.1074/mcp.M113.035600.

Huang, F., Wong, X., and Jan, L.Y. (2012). "International Union of Basic and Clinical Pharmacology. LXXXV: calcium-activated chloride channels". Pharmacological reviews *64*, 1-15. 10.1124/pr.111.005009.

Ito, G., Okamoto, R., Murano, T., Shimizu, H., Fujii, S., Nakata, T., Mizutani, T., Yui, S., Akiyama-Morio, J., Nemoto, Y., et al. (2013). "Lineage-specific expression of bestrophin-2 and bestrophin-4 in human intestinal epithelial cells". PLoS One *8*, e79693. 10.1371/journal.pone.0079693.

Katoh, M., and Katoh, M. (2004). "Identification and characterization of human HES2, HES3, and HES5 genes in silico". International journal of oncology *25*, 529-534.

Li, X., Hu, W., Zhou, J., Huang, Y., Peng, J., Yuan, Y., Yu, J., and Zheng, S. (2017). "CLCA1 suppresses colorectal cancer aggressiveness via inhibition of the Wnt/beta-catenin signaling pathway". Cell communication and signaling : CCS *15*, 38. 10.1186/s12964-017-0192-z.

M. B. Amin et al. (Springer, 2017). "AJCC Cancer Staging Manual".

Marmorstein, A.D., Cross, H.E., and Peachey, N.S. (2009). "Functional roles of bestrophins in ocular epithelia". Progress in retinal and eye research *28*, 206-226. 10.1016/j.preteyeres.2009.04.004.

Matchkov, V.V., Larsen, P., Bouzinova, E.V., Rojek, A., Boedtkjer, D.M., Golubinskaya, V., Pedersen, F.S., Aalkjaer, C., and Nilsson, H. (2008). "Bestrophin-3 (vitelliform macular dystrophy 2-like 3 protein) is essential for the cGMP-dependent calcium-activated chloride conductance in vascular smooth muscle cells". Circ Res *103*, 864-872. 10.1161/circresaha.108.178517.

Meng, J., Chen, S., Han, J.X., Qian, B., Wang, X.R., Zhong, W.L., Qin, Y., Zhang, H., Gao, W.F., Lei, Y.Y., et al. (2018). "Twist1 Regulates Vimentin through Cul2 Circular RNA to Promote EMT in Hepatocellular Carcinoma". Cancer research *78*, 4150-4162. 10.1158/0008-5472.Can-17-3009.

Milenkovic, V.M., Langmann, T., Schreiber, R., Kunzelmann, K., and Weber, B.H. (2008). "Molecular evolution and functional divergence of the bestrophin protein family". BMC evolutionary biology *8*, 72. 10.1186/1471-2148-8-72.

Miller, A.N., Vaisey, G., and Long, S.B. (2019). "Molecular mechanisms of gating in the calcium-activated chloride channel bestrophin". eLife *8*. 10.7554/eLife.43231.

Miotto, B., and Struhl, K. (2006). "Differential gene regulation by selective association of transcriptional coactivators and bZIP DNA-binding domains". Molecular and cellular biology *26*, 5969-5982. 10.1128/MCB.00696-06.

Murato, Y., and Hashimoto, C. (2009). "Xhairy2 functions in Xenopus lens development by regulating p27(xic1) expression". Developmental dynamics : an official publication of the American Association of Anatomists *238*, 2179-2192. 10.1002/dvdy.21883.

Nagai, T., Arao, T., Nishio, K., Matsumoto, K., Hagiwara, S., Sakurai, T., Minami, Y., Ida, H., Ueshima, K., Nishida, N., et al. (2016). "Impact of Tight Junction Protein ZO-1 and TWIST Expression on Postoperative Survival of Patients with Hepatocellular Carcinoma". Digestive diseases (Basel, Switzerland) *34*, 702-707. 10.1159/000448860.

Nichane, M., de Crozé, N., Ren, X., Souopgui, J., Monsoro-Burq, A.H., and Bellefroid, E.J. (2008). "Hairy2-Id3 interactions play an essential role in Xenopus neural crest progenitor specification". Developmental biology *322*, 355-367. 10.1016/j.ydbio.2008.08.003.

Parikh, K., Antanaviciute, A., Fawkner-Corbett, D., Jagielowicz, M., Aulicino, A., Lagerholm, C., Davis, S., Kinchen, J., Chen, H.H., Alham, N.K., et al. (2019). "Colonic epithelial cell diversity in health and inflammatory bowel disease". Nature *567*, 49-55. 10.1038/s41586-019-0992-y.

Pastushenko, I., and Blanpain, C. (2019). "EMT Transition States during Tumor Progression and Metastasis". Trends in cell biology *29*, 212-226. 10.1016/j.tcb.2018.12.001.

Pifferi, S., Dibattista, M., Sagheddu, C., Boccaccio, A., Al Qteishat, A., Ghirardi, F., Tirindelli, R., and Menini, A. (2009). "Calcium-activated chloride currents in olfactory sensory neurons from mice lacking bestrophin-2". The Journal of physiology *587*, 4265-4279. 10.1113/jphysiol.2009.176131.

Porretti, J., Dalton, G.N., Massillo, C., Scalise, G.D., Farré, P.L., Elble, R., Gerez, E.N., Accialini, P., Cabanillas, A.M., Gardner, K., et al. (2018). "CLCA2 epigenetic regulation by CTBP1, HDACs, ZEB1, EP300 and miR-196b-5p impacts prostate cancer cell adhesion and EMT in metabolic syndrome disease". International journal of cancer *143*, 897-906. 10.1002/ijc.31379.

Qu, H., Su, Y., Yu, L., Zhao, H., and Xin, C. (2019). "Wild-type p53 regulates OTOP2 transcription through DNA loop alteration of the promoter in colorectal cancer". FEBS open bio *9*, 26-34. 10.1002/2211-5463.12554.

Rawla, P., Sunkara, T., and Barsouk, A. (2019). "Epidemiology of colorectal cancer: incidence, mortality, survival, and risk factors". Przeglad gastroenterologiczny *14*, 89-103. 10.5114/pg.2018.81072.

Roger, L., Jullien, L., Gire, V., and Roux, P. (2010). "Gain of oncogenic function of p53 mutants regulates E-cadherin expression uncoupled from cell invasion in colon cancer cells". Journal of cell science *123*, 1295-1305. 10.1242/jcs.061002.

Sanders, K.M., Zhu, M.H., Britton, F., Koh, S.D., and Ward, S.M. (2012). "Anoctamins and gastrointestinal smooth muscle excitability". Exp Physiol *97*, 200-206. 10.1113/expphysiol.2011.058248.

Sui, Y., Sun, M., Wu, F., Yang, L., Di, W., Zhang, G., Zhong, L., Ma, Z., Zheng, J., Fang, X., and Ma, T. (2014). "Inhibition of TMEM16A expression suppresses growth and invasion in human colorectal cancer cells". PLoS One *9*, e115443. 10.1371/journal.pone.0115443.

Sun, L., Ke, J., He, Z., Chen, Z., Huang, Q., Ai, W., Wang, G., Wei, Y., Zou, X., Zhang, S., et al. (2017). "HES1 Promotes Colorectal Cancer Cell Resistance To 5-Fu by Inducing Of EMT and ABC Transporter Proteins". Journal of Cancer *8*, 2802-2808. 10.7150/jca.19142.

Sunlin Yong, Z.W., Tang Yuan, Chuang Cheng, Dan Jiang (2021). "Comparison of MMR protein and Microsatellite Instability Detection in Colorectal Cancer and Its Clinicopathological Features Analysis". Journal of Medical Research *50*, 61-66. 10.11969/j.issn.1673-548X.2021.05.015

Tsunenari, T., Sun, H., Williams, J., Cahill, H., Smallwood, P., Yau, K.W., and Nathans, J. (2003). "Structure-function analysis of the bestrophin family of anion channels". The Journal of biological chemistry *278*, 41114-41125. 10.1074/jbc.M306150200.

van Es, J.H., van Gijn, M.E., Riccio, O., van den Born, M., Vooijs, M., Begthel, H., Cozijnsen, M., Robine, S., Winton, D.J., Radtke, F., and Clevers, H. (2005). "Notch/gamma-secretase inhibition turns proliferative cells in intestinal crypts and adenomas into goblet cells". Nature *435*, 959-963. 10.1038/nature03659.

Vesuna, F., van Diest, P., Chen, J.H., and Raman, V. (2008). "Twist is a transcriptional repressor of E-cadherin gene expression in breast cancer". Biochem Biophys Res Commun *367*, 235-241. 10.1016/j.bbrc.2007.11.151.

Walia, V., Yu, Y., Cao, D., Sun, M., McLean, J.R., Hollier, B.G., Cheng, J., Mani, S.A., Rao, K., Premkumar, L., and Elble, R.C. (2012). "Loss of breast epithelial marker hCLCA2 promotes epithelial-to-mesenchymal transition and indicates higher risk of metastasis". Oncogene *31*, 2237-2246. 10.1038/onc.2011.392.

Wang, Z., Kawaguchi, K., Honda, M., Hashimoto, S., Shirasaki, T., Okada, H., Orita, N., Shimakami, T., Yamashita, T., Sakai, Y., et al. (2019). "Notch signaling facilitates hepatitis B virus covalently closed circular DNA transcription via cAMP response element-binding protein with E3 ubiquitin ligase-modulation". Scientific reports *9*, 1621. 10.1038/s41598-018-38139-5.

Yang, B., Cao, L., Liu, J., Xu, Y., Milne, G., Chan, W., Heys, S.D., McCaig, C.D., and Pu, J. (2015). "Low expression of chloride channel accessory 1 predicts a poor prognosis in colorectal cancer". Cancer *121*, 1570-1580. 10.1002/cncr.29235.

Yang, J., Mani, S.A., Donaher, J.L., Ramaswamy, S., Itzykson, R.A., Come, C., Savagner, P., Gitelman, I., Richardson, A., and Weinberg, R.A. (2004). "Twist, a master regulator of morphogenesis, plays an essential role in tumor metastasis". Cell *117*, 927-939. 10.1016/j.cell.2004.06.006.

Yeung, K.T., and Yang, J. (2017). "Epithelial-mesenchymal transition in tumor metastasis". Molecular oncology *11*, 28-39. 10.1002/1878-0261.12017.

Yu, X., Li, S., Xu, Y., Zhang, Y., Ma, W., Liang, C., Lu, H., Ji, Y., Liu, C., Chen, D., and Li, J. (2020). "Androgen Maintains Intestinal Homeostasis by Inhibiting BMP Signaling via Intestinal Stromal Cells". Stem cell reports *15*, 912-925. 10.1016/j.stemcr.2020.08.001.

Yuan, R., Ke, J., Sun, L., He, Z., Zou, Y., He, X., Chen, Y., Wu, X., Cai, Z., Wang, L., et al. (2015). "HES1 promotes metastasis and predicts poor survival in patients with colorectal cancer". Clinical & experimental metastasis *32*, 169-179. 10.1007/s10585-015-9700-y.

Yusup, A., Huji, B., Fang, C., Wang, F., Dadihan, T., Wang, H.J., and Upur, H. (2017). "Expression of trefoil factors and TWIST1 in colorectal cancer and their correlation with metastatic potential and prognosis". World journal of gastroenterology *23*, 110-120. 10.3748/wjg.v23.i1.110.

Zhang, L., Cao, F., Zhang, G., Shi, L., Chen, S., Zhang, Z., Zhi, W., and Ma, T. (2019). "Trends in and Predictions of Colorectal Cancer Incidence and Mortality in China From 1990 to 2025". Frontiers in oncology *9*, 98. 10.3389/fonc.2019.00098.

Zhang, N., Ng, A.S., Cai, S., Li, Q., Yang, L., and Kerr, D. (2021). "Novel therapeutic strategies: targeting epithelial-mesenchymal transition in colorectal cancer". The Lancet. Oncology *22*, e358-e368. 10.1016/s1470-2045(21)00343-0.

Zhu, D.J., Chen, X.W., Zhang, W.J., Wang, J.Z., Ouyang, M.Z., Zhong, Q., and Liu, C.C. (2015). "Twist1 is a potential prognostic marker for colorectal cancer and associated with chemoresistance". American journal of cancer research *5*, 2000-2011.

Figure legends

Figure 1. *BEST4* inhibits CRC cell proliferation, clonogenesis, migration, and invasion in vitro. Overexpression of *BEST4* decreased proliferation of HCT 116 (A) and Caco2 (B) cells as determined by the IncuCyte confluence assay. (C) Viability of three individual *BEST4*-deleted clones as determined by a CCK-8 assay. (D) *BEST4* deletion significantly enhanced cell viability compared with cells transduced with EV-gRNA control; the reintroduction of *BEST4* resulted in suppressed cell growth as determined by IncuCyte confluence analysis. (E) Expression of *BEST4*-HA in HCT116 and Caco2 cells resulted in more colonies than cells transduced with EV plasmids (left panel); colonies were counted and analysed as shown (right panel). (F) A colony formation assay was performed to evaluate the responses of HCT-15 cells following *BEST4* deletion and reintroduction (left panel); cell colonies were counted and analysed as shown (right panel). (G) Heterologous expression of BEST4 in HCT116 cells suppressed invasion and migration (upper panel, scale bar, 200 μm); cells that passed

through the membrane were counted and compared (lower panel). (H) *BEST4* deletion in HCT-15 cells promoted invasion, whereas reintroduction of *BEST4* expression resulted in the inhibition of HCT-15 cell invasion and migration (upper panel, scale bar, 200 μm). Cells that passed through the membrane were counted and compared (lower panel). Data shown are the result of at least three independent experiments, with the mean ± SEM; **P*<0.05, ***P*<0.01 vs EV or WT.

Figure 2. *BEST4* deters EMT in CRC in vitro and *in vivo*. (A) Expression of mRNAs encoding EMT-related genes as determined by qPCR in HCT116 cells transfected with BEST4-HA or EV. (B) As determined by qPCR, the expression of mRNAs encoding EMT markers in *BEST4*-deleted and *BEST4*-restored HCT-15 cells. (C) Protein expression of EMT-related genes was evaluated by western blotting of lysates of HCT116 cells transfected with BEST4-HA or EV. (D) Western blotting determined the levels of immunoreactive EMT markers in *BEST4*-deleted and *BEST4*-restored HCT-15 cells. (E) Growth of xenograft tumours in BALB/c nude mice resulting from the injection of HCT116 cells stably-transduced with *BEST4*-HA was significantly diminished compared with those resulting from HCT116 cells transduced with EV alone (eight mice per group). (F) The histogram represents the mean weights of tumours isolated from the HCT116-*BEST4*-HA and HCT116-EV groups. (G) Tumours from the HCT116-*BEST4*-HA and HCT116-EV groups were sectioned and subjected to immunohistochemical staining to detect HA and human Ki67; scale bar=50 μm. (H) Mean percentage of Ki67-positive staining in each group. (I) Representative western blot documenting protein levels of EMT markers in individual HCT116-BEST4 and HCT116-EV xenograft tumours. **P*<0.05, ***P*<0.01. Data from at least three independent experiments are presented as the mean ± SEM. (J-L) Intrasplenical injections of HCT-15 cell lines with EV-gRNA control, BEST4-gRNA or BEST4-Rescued (n = 3 per

group). After 28 days, the animals were sacrificed and numbers of metastatic nodules in the liver were counted, and the liver tissues were fixed for sectioning and H&E staining; T, Tumour.Data are presented as the mean ± SEM. ***P*<0.01 vs EV-gRNA.

Figure 3. Molecular regulation of BEST4 expression by Hes4. (A) Endogenous *BEST4* mRNA and protein levels in *Hes4*-overexpressing HCT116 cells were detected by qPCR and western blotting, respectively. (B) Endogenous *BEST4* mRNA and protein levels in LS174T cells after shRNA-mediated Hes4 knockdown as detected by qPCR and western blotting, respectively. (C) Detection of *BEST4* promoter activity in Hes4-overexpressing HCT116 cells using a dual-luciferase reporter assay. (D) As determined by ChIP-qPCR, Fold-enrichment of the *BEST4* promoter region in Flag-ChIP samples from Hes4-overexpressing HCT116 cells. Data were normalized using a fold-enrichment method (i.e., ChIP signals divided by control IgG signals). The DHFR 5' UTR was used as a negative control (upper panel). The primer sets that target the BEST4 promoter in the ChIP-qPCR assays are as illustrated; +1 marks the transcriptional start site of *BEST4*, and P1, P2, P3, and P4 represent primer locations (lower panels). (E) Immunofluorescence staining documents the colocalization of BEST4 (green) and Hes4 (red) in HCT116 cells based on detection of their specific tags; scale bar, 20 μM. (F) Co-immunoprecipitation of nuclear extracts with specifically-tagged BEST4 and Hes4 as determined by immunoblotting. Lamin B1 served as a nuclear protein control. (G) Detection of *BEST4* promoter activity in *Hes4*-overexpressing HCT116 cells after *BEST4* knockdown through a dual-luciferase reporter assay. Data shown are the result of at least three independent experiments, with the mean ± SEM; **P*<0.05, ***P*<0.01 vs EV

Figure 4. *BEST4* relays the Hes4 signal and downregulates Twist1 expression to counteract EMT induction in CRC (A) Detection of Twist1 promoter activity in *Hes4*-overexpressing or *BEST4*-overexpressing HCT116 cells through a dual-luciferase reporter assay. (B) Detection of Twist1 promoter activity in *Hes4*-overexpressing HCT116 cells after BEST4 knockdown through a dual-luciferase reporter assay. (C) Detection of Twist1 promoter activity in HCT116 cells after shRNA-mediated Hes4 knockdown and combination with *BEST4*-overexpressing using a dual-luciferase reporter assay. (D) Co-immunoprecipitation of nuclear extracts with specifically-tagged BEST4 and Twist1 as determined by immunoblotting. Lamin B1 served as a nuclear protein control. (E) Co-immunoprecipitation of nuclear extracts with specifically-tagged Hes4 and Twist1 as determined by immunoblotting. Lamin B1 served as a nuclear protein control. (F) Expression of EMT markers in *Hes4*-overexpressing HCT116 cells. (G) Expression of EMT markers in LS174T cells after shRNA-mediated *Hes4* knockdown. (H) Expression of EMT markers in *Hes4*-overexpressing HCT116 cells after BEST4 knockdown. (I) Expression levels of EMT markers in *BEST4*-overexpressing LS174T cells after Hes4-knockdown; SCR, scrambled siRNA.

Figure 5. Correlation of the *BEST4* mRNA expression with clinicopathology and outcomes of patients diagnosed with CRC. (A) Heatmap based on the top 100 differentially expressed genes (downregulated and upregulated) in CRCs compared with ANTs. (B) Volcano plots of RNA seq results showing all differentially expressed genes in CRC tissues compared with ANTs based on the fold-change ($|FC| \geq 1$) and *P-value* ($P \leq 0.05$). (C) Expression levels of *BEST4* mRNA in 50 pairs of adenoma tissues compared with ANTs. (D) Expression levels of *BEST4* mRNA in 124 pairs of CRC tissues compared with ANTs. (E) BEST4 protein levels in CRC and their matched counterparts were measured using western blotting.

(F) Kaplan-Meier survival analysis according to *BEST4* expression in 124 patients with CRC. The difference was statistically significant based on the log-rank test ($P<0.01$). (G) A working model delineates the mechanism by which *BEST4* is transcriptionally activated by *Hes4* and suppressed EMT through Twist1 inhibition: a. the expression of *BEST4* is regulated by interactions of its upstream promoter region with Hes4. *BEST4* positively promotes the transcriptional activity of Hes4 on *BEST4* by physically binding to Hes4 in a positive feedback loop; b. The complex formed by BEST4 and Hes4 interacts with Twist1 and inhibits the promoter activity of Twist1. Hes4 alone is insufficient to inhibit Twist1 promoter activity, and BEST4 is required. Inhibition of Twist1 promoter activity by Hes4 is BEST4-dependent c. The complex formed by BEST4 and Hes4 destabilized Twist1; the same effect caused by Hes4 required BEST4 intermediation. The Hes4-BEST4-Twist1 axis counteracts EMT induction. *$P<0.05$, **$P<0.01$; CRC, colorectal cancer; ANT, adjacent normal tissue; T, tumour.

Figure Supplement Legends

Figure 1-supplemental figure 1. Construction of *BEST4*-overexpressing /*BEST4*-depetion CRC cell lines, and cell proliferation measured by CCK-8 assay. (A) HA protein expression in *BEST4*-HA-transfected GFP^+ HCT116 individual clonal lines. (B) HA protein expression in *BEST4*-HA-transfected GFP^+ Caco2 individual clonal lines. (C) *BEST4* mRNA and HA protein expression was detected by real-time PCR and western blotting. (D) Cell viability in *BEST4*-HA- and EV-transfected HCT116 cells was measured by the CCK-8 assay. (E) Cell viability in *BEST4*-HA- and EV-transfected Caco2 cells was measured by the CCK-8 assay. (F) DNA sequencing results revealed an excision of a 44-bp genomic fragment in exon 3 of the *BEST4*-knockout lines. (G) DNA

fragmentation from each sample was analysed by agarose gel electrophoresis. (H) The protein level of BEST4 was determined by western blotting. (H) Cell proliferation measured by CCK-8 assay showed that knockout of *BEST4* obviously promoted cell growth; however, rescue of *BEST4* expression in the knockout cells significantly abrogated the promotive effect of *BEST4* knockout on cell growth. *P<0.05, **P<0.01. All the data come from three independent experiments and are presented as the mean ± standard deviation.

Figure 2-supplemental figure 1. Western blot signals were quantified using ImageJ software. (A-D) Each band's mean pixel intensities were determined and normalized to mean β-actin pixel intensity. $^{*}P<0.05$, $^{**}P<0.01$. Data from at least three independent experiments are presented as the mean ± SEM.

Figure 3-supplemental figure 1. *BEST4* interacted with *Hes4*. (A) *Hes4* mRNA level in each CRC cell line. (B) Western blot for BEST4 expression of Figure 3A is quantified by ImageJ, each band's mean pixel intensities were determined and normalized to mean β-actin pixel intensity. (C) *Hes4* mRNA and protein levels in HCT116 cells with *Hes4* overexpression by Flag-*Hes4* transfection were examined by real-time PCR and western blot. (D) Western blot for BEST4 expression of Figure 3B is quantified by ImageJ, each band's mean pixel intensities were determined and normalized to mean β-actin pixel intensity. (E) *Hes4* mRNA and protein levels in LS174T cells with *Hes4* knockdown by shRNA transfection were examined by real-time PCR and western blot. (F) No significant change of *Hes4* mRNA levels in *BEST4*-overexpression HCT116 cells as detected by real-time PCR. *P<0.05, **P<0.01. All the data come from three independent experiments and are presented as the mean ± SEM.

SRC, scramble siRNA.

Figure 4-supplemental figure 1. *BEST4* interacted with *Hes4* to inhibit Twist1. (A) *BEST4* mRNA levels in HCT116 and LS174T cells transfected with *BEST4*-specific siRNAs as detected by real-time PCR. (B) Co-immunoprecipitation of nuclear extracts with specifically-tagged BEST4 and Twist1 as determined by immunoblotting, Lamin B1 served as a nuclear protein control. (C) Co-immunoprecipitation of nuclear extracts with specifically-tagged Hes4 and Twist1 as determined by immunoblotting, Lamin B1 served as a nuclear protein control. (D) *Vimentin* mRNA levels in *Hes4*-overexpression HCT 116 cell lines as detected by real-time PCR. (E) *Vimentin* mRNA levels in *Hes4*-overexpression HCT 116 cell lines after *BEST4* knockdown as detected by real-time PCR. $^{*}P<0.05$, $^{**}P<0.01$. All the data were generated from three independent experiments and are presented as the mean ± SEM. SRC, scramble siRNA.

Figure 4-supplemental figure 2. Western blot signals were quantified using ImageJ software. (A-D) Each band's mean pixel intensities were determined and normalized to mean β-actin pixel intensity. $^{*}P<0.05$, $^{**}P<0.01$. Data from at least three independent experiments are presented as the mean ± SEM.

Figure 5-supplemental figure 1. *BEST4* suppresses EMT independently of its channel functions. (A-C) Incubation of HCT116 cell lines expressed BEST4 or EV with DIDS (300μM), a gradient increased CaCCinh-A01 and ionomycin (1μM), respectively, overnight. The levels of chloride efflux were determined by calculating relative fold to the EV control. Data are shown as means ± SEM, $p < 0.05$ vs EV or DIDS, or CaCCinh-A01 or ionomycin, with 3 independent experiments. (D-F) Following the

same treatment, cell lysates were prepared for immunoblotting with antibodies to BEST4, ZO-1, E-cadherin, Twist1 and β-actin. Representative 3 independent experiments. (G) Western blot for BEST4 expression of Figure 5E is quantified by ImageJ, each band's mean pixel intensities were determined and normalized to mean β-actin pixel intensity. *P<0.05, **P<0.01. Data from at least three independent experiments are presented as the mean ± SEM

Figure 6-supplemental figure 1. *BEST4* mRNA expression in colorectal tumours and matched non-tumour tissues and the clinical relationship between *BEST4*, *Hes4* and EMT markers. (A) Correlation between *BEST4* and *CDH1* in normal and colorectal cancer samples analysed from the TCGA and GTEx databases using the GEPIA tool (http://gepia.cancer-pku.cn/). (B) RNA-seq data revealed decreased expression of and *Hes4* in CRC tissues compared with ANTs. (C) Heatmap of *Hes4* expression in CRC and ANTs. (D) The correlation between *BEST4* and *Hes4*, in CRC analysed from the TCGA and GTEx databases using GEPIA (http://gepia.cancer-pku.cn/). (E) Correlation between *BEST4* and *CDH1* in normal and colorectal cancer samples analysed from the TCGA and GTEx databases using the GEPIA tool (http://gepia.cancer-pku.cn/). (F) Correlation between *BEST4* and *vimentin* in normal and colorectal cancer samples. (G) Correlation between *BEST4* and Twist1 in normal and cancer colorectal samples. ANT, adjacent normal tissues; COAD, colon adenocarcinoma; READ, rectum adenocarcinoma; other tumour abbreviations are available at GEPIA: http://gepia.cancer-pku.cn/.

Key resources table

REAGENT or RESOURCE	SOURCE	IDENTIFIER

Antibodies		
BEST4	LsBio	Cat# LS-C31133-100, RRID:AB_911624
Hes4	Santa Cruz	Cat# sc-376002, RRID:AB_10987629
Flag	Sigma-Aldrich	Cat# F3165, RRID:AB_259529)
HA	Cell Signaling Technology	Cat# 3724, RRID:AB_1549585
ZO-1	Cell Signaling Technology	Cat# 8193, RRID:AB_10898025
E-Cadherin	Cell Signaling Technology	Cat# 3195, RRID:AB_2291471
Vimentin	Cell Signaling Technology	Cat# 5741, RRID:AB_1069545
Twist1	Cell Signaling Technology	Cat# 46702, RRID:AB_279930
Mouse (G3A1) mAb IgG1	Cell Signaling Technology	Cat# 5415, RRID:AB_10829607
Normal rabbit IgG	Cell Signaling Technology	Cat# 2729, RRID:AB_103106

Ki-67	Cell Signaling Technology	Cat# 9449, RRID:AB_2797703
Alexa Fluor 647	Invitrogen	Cat# A-21235, RRID:AB_2535804
TRITC	Abcam	Cat# ab6718, RRID:AB_955551
Anti-rabbit IgG	Cell Signaling Technology	Cat# 14708, RRID:AB_2798581
Anti-mouse IgG	Cell Signaling Technology	Cat# 14709, RRID:AB_2798582
HRP-conjugated secondary antibody	Dako	Cat# P0447, RRID:AB_2617137
β-actin	Cell Signaling Technology	Cat# 3700, RRID:AB_2242334
Lamin B1	Cell Signaling Technology	Cat# 17467, RRID:AB_ 10896336
Biological samples		
Human colorectal cancer samples	West China Hospital of Sichuan University	N/A
Chemicals, peptides, and recombinant proteins		
Direct-zol RNA Kit	Zymo Research	Cat# R2050

High-Capacity cDNA Reverse Transcription Kit	Thermo Fisher Scientific	Cat# 4368814
SYBR Green	Bioline Reagents Ltd,	Cat# RR036A
RIPA lysis buffer	Merck Millipore	Cat# P0013B
protease inhibitor cocktail	Sigma-Aldrich	Cat# P8340
phosphatase inhibitor	Sigma-Aldrich	Cat# P5726
Matrigel	BD Biosciences	Cat# 356234
Protein G Dynabeads	Thermo Fisher Scientific	Cat# 1009D
Protein A/G Magnetic Beads	MedChemExpress,	Cat# HY-K0202
DMEM	GIBCO Thermo Fisher Scientific	Cat# 31966
FBS	GIBCO Thermo Fisher Scientific	Cat# 10270
Lipofectamine 3000	Invitrogen	Cat# L3000001
puromycin	Invivogen	Cat# anti-pr
Critical commercial assays		
Cell Counting Kit-8 (CCK-8) assay	Dojindo	Cat# CK04

Protein assay kit	Bio-Rad,	Cat# 5000001
Dual-Luciferase Reporter Assay System	Promega	Cat #E1910
MycoAlert™ Mycoplasma Detection Kit	Lonza	Cat# LT07-318
Minute™ Cytoplasmic and Nuclear Fractionation Kit	Invent	Cat# SC-003
Deposited data		
RNA-seq data	NCBI SRA	RJNA690126
Experimental models: Cell lines and animals		
HCT116	ATCC	Cat# CCL-247
Caco2	ATCC	Cat# HTB-37
HCT-15	ATCC	Cat# CCL-225,
LS174T	ATCC	Cat# CCL-188
HEK293T	ATCC	Cat# CRL3216
BALB/c nude mice	Beijing HFK Bioscien ce	N/A
Oligonucleotides		
qPCR Primer sequences	See Table S1	N/A
shRNA sequences	See Table S1	N/A

siRNA sequences	See Table S1	N/A
ChIP-qPCR Primer sequences	See Table S1	N/A
Recombinant DNA		
Plasmid: pCDH-CMV-MCS-EF1-CopGFP-T2A-Puro	Public Protein/Plasmid Library	Cat# 030001
Plasmid: BEST4-HA-GFP	Public Protein/Plasmid Library	Cat# PPL01999-4b
Plasmid: pU6-gRNA-Cas9-EGFP	GenePharma	Cat# B5620
Plasmid: BEST4-gRNA	GenePharma	Cat# B5620
Plasmid: Flag-Hes4-GFP	Public Protein/Plasmid Library	Cat# PPL01973-4a
Plasmid: pGL3-basic vectors	Promega	Cat# E1751
Plasmid: pRL-TK	Promega	Cat# E2241
Plasmid: pGL3-BEST4	Public Protein/Plasmid Library	Cat# PPL01999-2a
Plasmid: pcDNA3.1	Public Protein/Plasmid Library	Cat# PE004
Plasmid: HES4-shRNA	Public Protein/Plasmid Library	Cat# PPL01973-3

Software and algorithms		
IncuCyte software	This paper	https://www.essenbioscience.com/
ImageJ	This paper	https://imagej.nih.gov/ij/
SPSS 25.0	This paper	www.ibm.com/software/analytics/spss

Figure 1

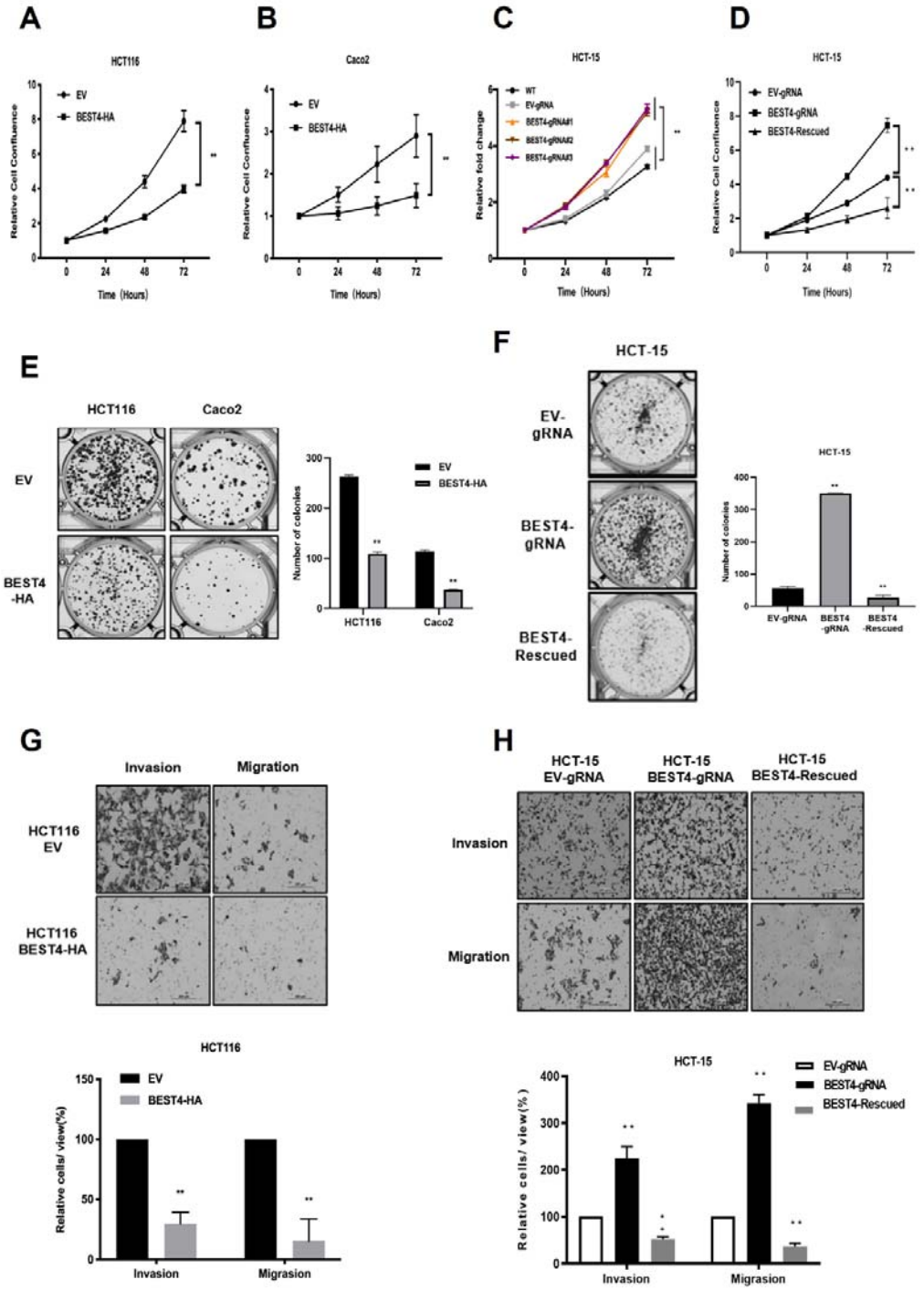
A
HCT116
EV
BEST4-HA
Relative Cell Confluence
Time (Hours)
B
Caco2
EV
BEST4-HA
Relative Cell Confluence
Time (Hours)
C
HCT-15
WT
EV-gRNA
BEST4-gRNA#1
BEST4-gRNA#2
BEST4-gRNA#3
Relative fold change
Time (Hours)
D
HCT-15
EV-gRNA
BEST4-gRNA
BEST4-Rescued
Relative Cell Confluence
Time (Hours)
E
HCT116
Caco2
EV
BEST4 -HA
Number of colonies
EV
BEST4-HA
HCT116
Caco2
F
HCT-15
EV-gRNA
BEST4-gRNA
BEST4-Rescued
HCT-15
Number of colonies
EV-gRNA
BEST4 -gRNA
BEST4 -Rescued
G
Invasion
Migration
HCT116 EV
HCT116 BEST4-HA
HCT116
EV
BEST4-HA
Relative cells/ view(%)
Invasion
Migrasion
H
HCT-15 EV-gRNA
HCT-15 BEST4-gRNA
HCT-15 BEST4-Rescued
Invasion
Migration
HCT-15
EV-gRNA
BEST4-gRNA
BEST4-Rescued
Relative cells/ view(%)
Invasion
Migrasion

877

878

879

Figure2

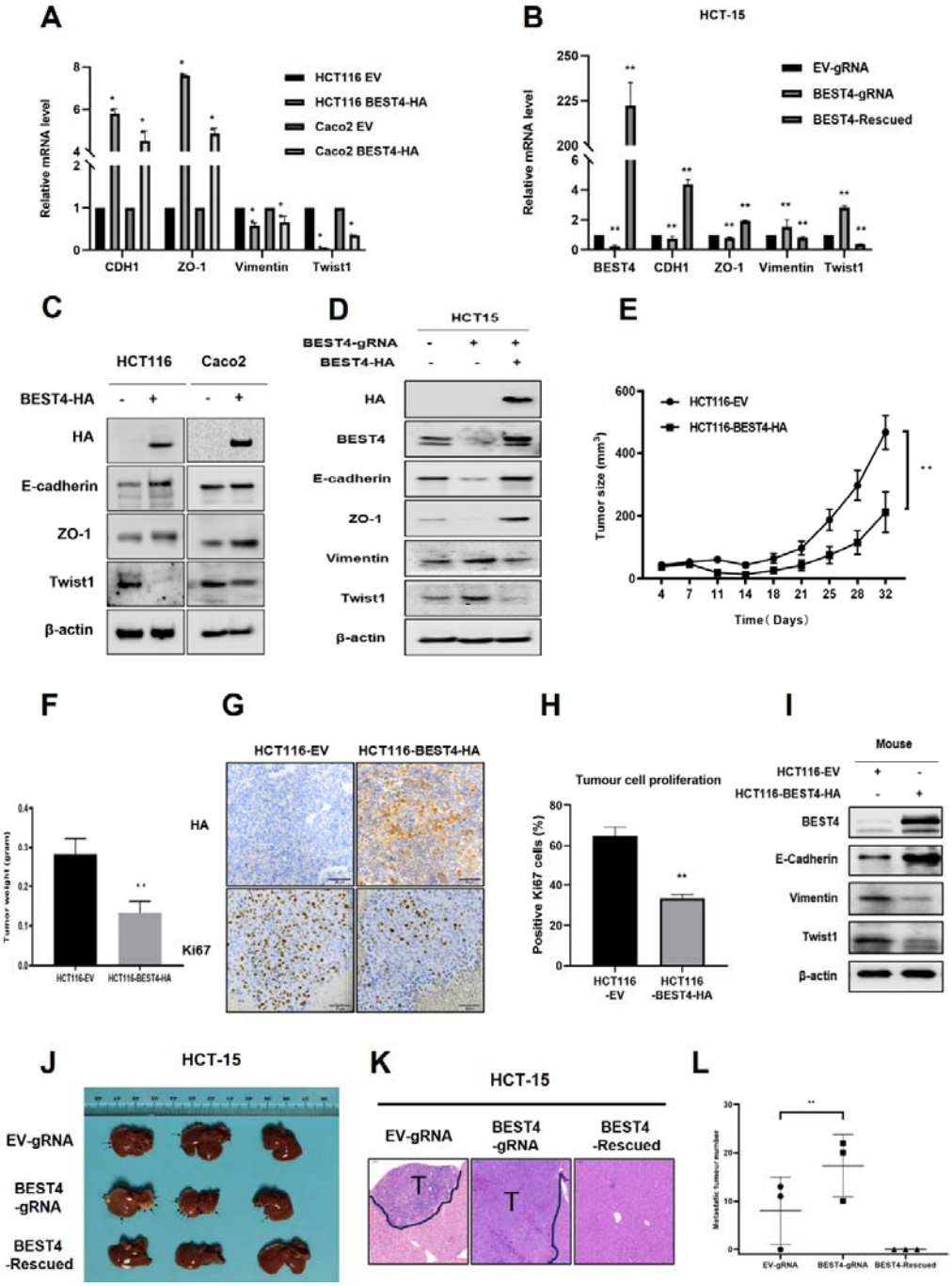
A
Relative mRNA level
HCT116 EV
HCT116 BEST4-HA
Caco2 EV
Caco2 BEST4-HA
CDH1
ZO-1
Vimentin
Twist1
B
HCT-15
EV-gRNA
BEST4-gRNA
BEST4-Rescued
BEST4
C
HCT116
Caco2
BEST4-HA
HA
E-cadherin
ZO-1
Twist1
β-actin
D
HCT15
BEST4-gRNA
BEST4-HA
E
HCT116-EV
HCT116-BEST4-HA
Tumor size (mm³)
Time（Days）
F
Tumor weight (grams)
G
HCT116-EV
HCT116-BEST4-HA
Ki67
H
Tumour cell proliferation
Positive Ki67 cells (%)
I
Mouse
J
HCT-15
K
L

Figure 3

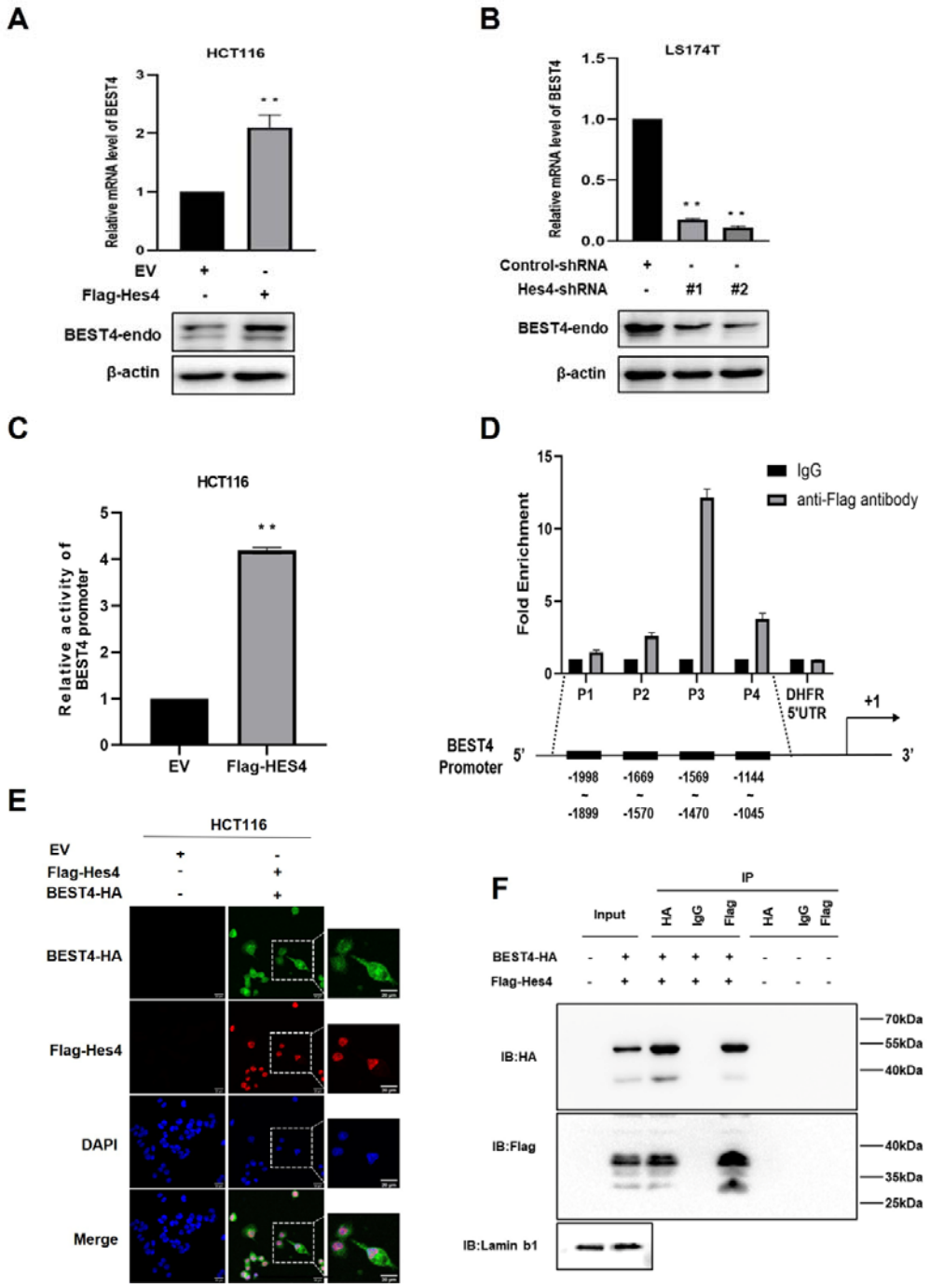
A
HCT116
Relative mRNA level of BEST4
EV
Flag-Hes4
BEST4-endo
β-actin
B
LS174T
Relative mRNA level of BEST4
Control-shRNA
Hes4-shRNA
#1
#2
BEST4-endo
β-actin
C
HCT116
Relative activity of BEST4 promoter
EV
Flag-HES4
D
IgG
anti-Flag antibody
Fold Enrichment
P1
P2
P3
P4
DHFR 5'UTR
+1
BEST4 Promoter
5'
3'
-1998 ~ -1899
-1669 ~ -1570
-1569 ~ -1470
-1144 ~ -1045
E
HCT116
EV
Flag-Hes4
BEST4-HA
DAPI
Merge
F
IP
Input
HA
IgG
Flag
BEST4-HA
Flag-Hes4
IB:HA
IB:Flag
IB:Lamin b1
70kDa
55kDa
40kDa
40kDa
35kDa
25kDa

Figure 4

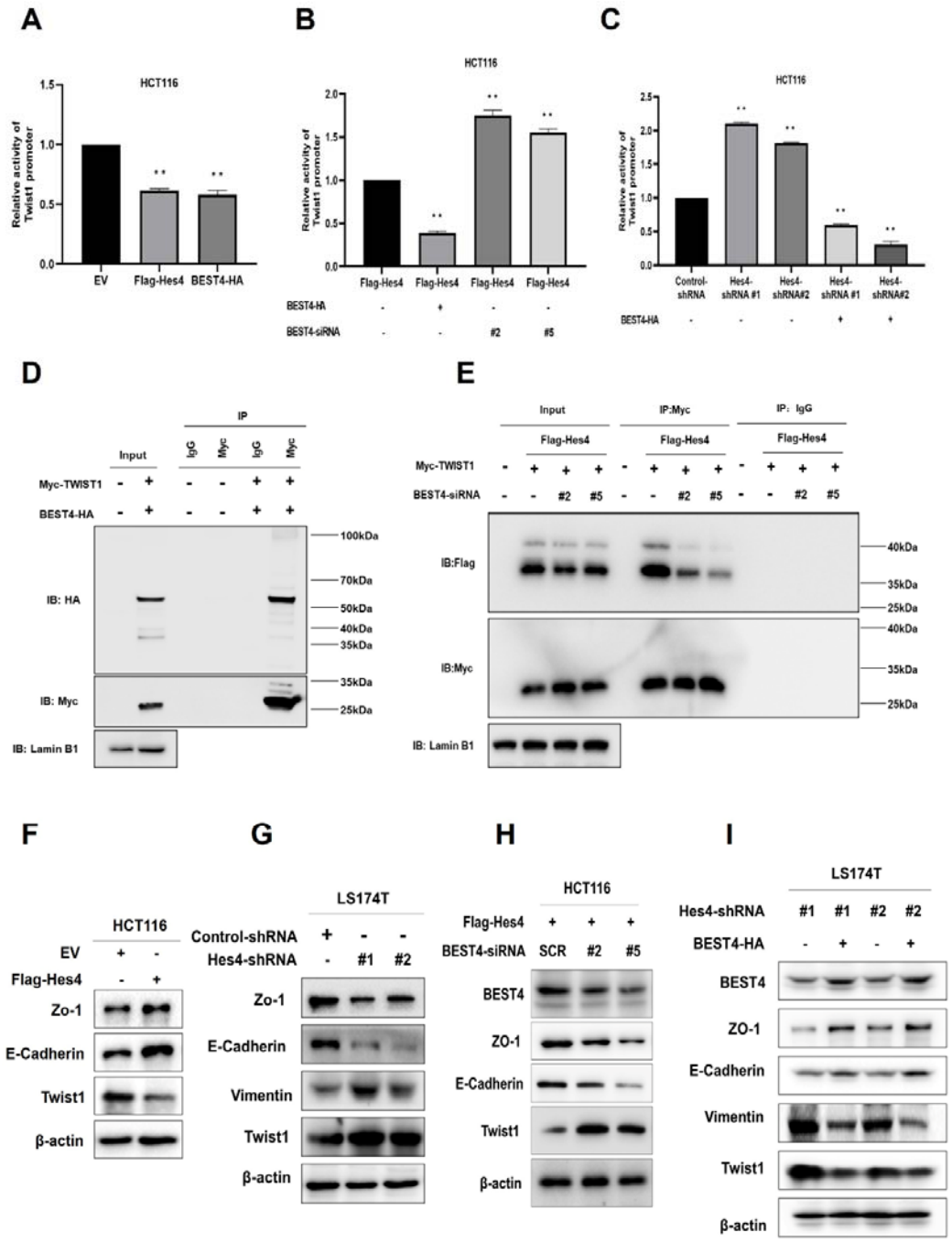
A
HCT116
Relative activity of Twist1 promoter
EV
Flag-Hes4
BEST4-HA
B
HCT116
Relative activity of Twist1 promoter
Flag-Hes4
BEST4-HA
BEST4-siRNA
#2
#5
C
HCT116
Relative activity of Twist1 promoter
Control-shRNA
Hes4-shRNA #1
Hes4-shRNA#2
BEST4-HA
D
IP
Input
IgG
Myc
Myc-TWIST1
BEST4-HA
IB: HA
IB: Myc
IB: Lamin B1
100kDa
70kDa
50kDa
40kDa
35kDa
25kDa
E
Input
IP:Myc
IP: IgG
Flag-Hes4
Myc-TWIST1
BEST4-siRNA
IB:Flag
IB:Myc
IB: Lamin B1
F
HCT116
EV
Flag-Hes4
Zo-1
E-Cadherin
Twist1
β-actin
G
LS174T
Control-shRNA
Hes4-shRNA
#1
#2
Zo-1
E-Cadherin
Vimentin
Twist1
β-actin
H
HCT116
Flag-Hes4
BEST4-siRNA
SCR
#2
#5
BEST4
ZO-1
E-Cadherin
Twist1
β-actin
I
LS174T
Hes4-shRNA
BEST4-HA
BEST4
ZO-1
E-Cadherin
Vimentin
Twist1
β-actin

Figure 5

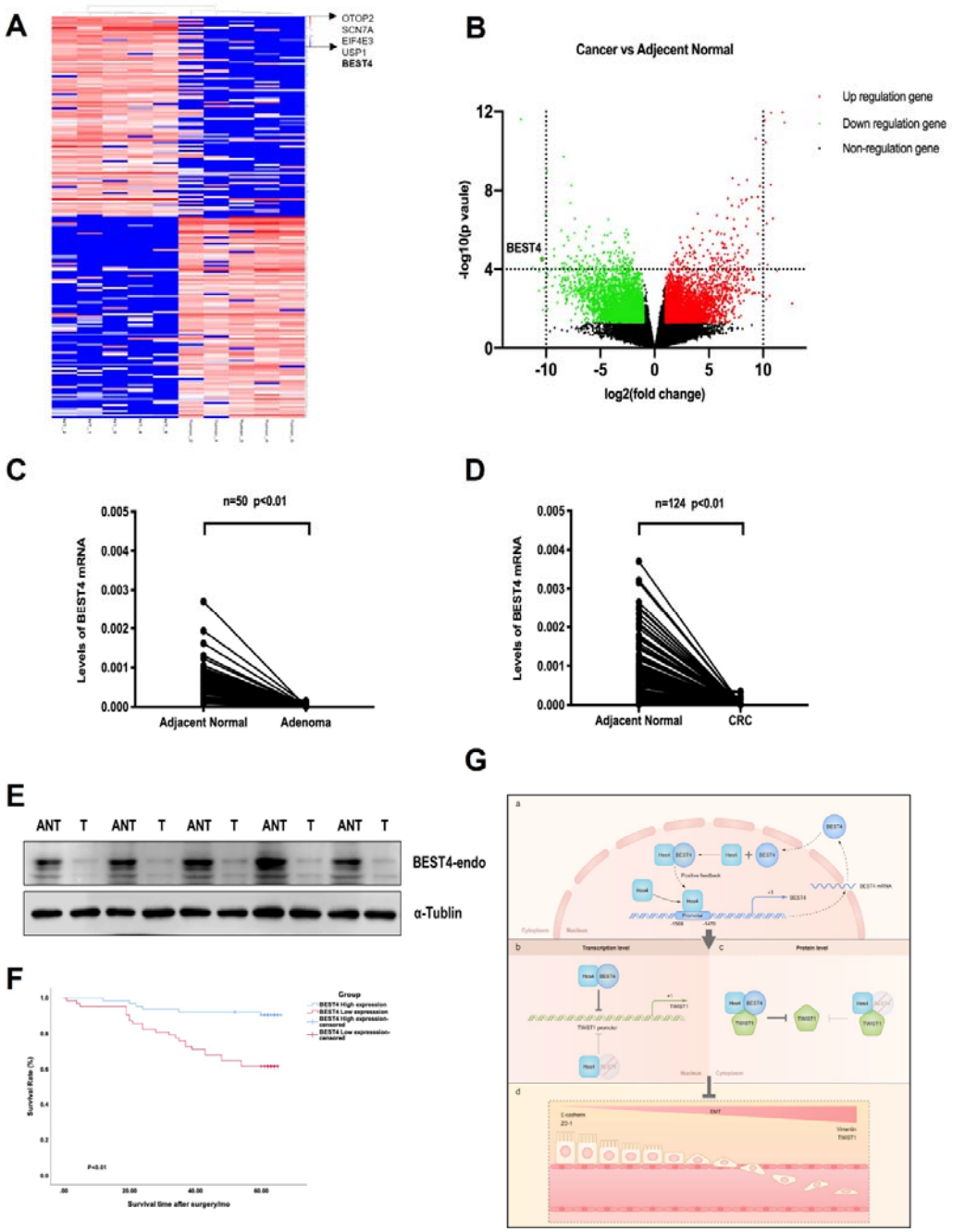
A
OTOP2
SCN7A
EIF4E3
USP1
BEST4
B
Cancer vs Adjecent Normal
Up regulation gene
Down regulation gene
Non-regulation gene
-log10(p vaule)
BEST4
log2(fold change)
C
n=50 p<0.01
Levels of BEST4 mRNA
Adjacent Normal
Adenoma
D
n=124 p<0.01
Levels of BEST4 mRNA
Adjacent Normal
CRC
E
ANT T ANT T ANT T ANT T ANT T
BEST4-endo
α-Tublin
F
Group
Survival time after surgery/mo
G

Table1. Correlation of *BEST4* mRNA level with clinicopathological factors.

Parameter	n	*BEST4* expression		P value
		Low	High	
Age (yr)				.66
<60	58	30	28	
≥60	67	32	35	
Sex				**.022***
Male	74	43	31	
Female	51	19	32	
Tumor differentiation				.258
Poor	10	3	7	
Moderate	114	59	55	
Well	1	0	1	
Tumor stage (TNM)[a]				
I	23	10	13	**.02***

II	50	18	32	
III	43	27	16	
IV	9	7	2	
Lymph node metastasis				**.032***
N0	75	30	45	
N1	41	26	15	
N2	9	6	3	
Distant metastasis				.08
Absent	116	55	61	
Present	9	7	2	
Location				.114
Colon	32	12	20	
Rectum	93	50	43	
CEA level				.13
Low	63	27	26	
High	62	35	27	

[a] Staging was performed according to the eighth edition of AJCC (M. B. Amin et al., Springer, 2017)

* Statistically significant.

Table 2. Univariate and Multivariate analysis of prognostic factors for overall survival of patients with CRC.

Variable	Comparison	Univariate analysis, P (log-rank test)	Multivariate analysis		
			HR	95%CI	P
Age (yr)	≥60 vs <60	**.001***	2.713	1.524-4.810	**.001***
Sex	female vs male	.681	NA	NA	NA
Clinical stage	II, III, IV vs I	.1	NA	NA	NA
Tumor differentiation	moderate, well vs poor	.08	NA	NA	NA
Lymph node metastasis	N1, N2 vs N0	**<0.001***	2.190	1.291-3.717	**.004***
Distant metastasis	present vs absent	**<0.001***	2.185	1.103-4.328	**.025***
Location	rectum vs colon	.22	NA	NA	NA
CEA level	high vs low	**.002***	1.697	0.953-2.960	**.073**
BEST4 level	high vs low	**<0.001***	.285	0.157-.606	**<0.001***

Abbreviations: HR, hazard ratio; CI, confidence interval; NA, not applicable.

□ Statistically significant.

Figure 1-supplemental figure 1.

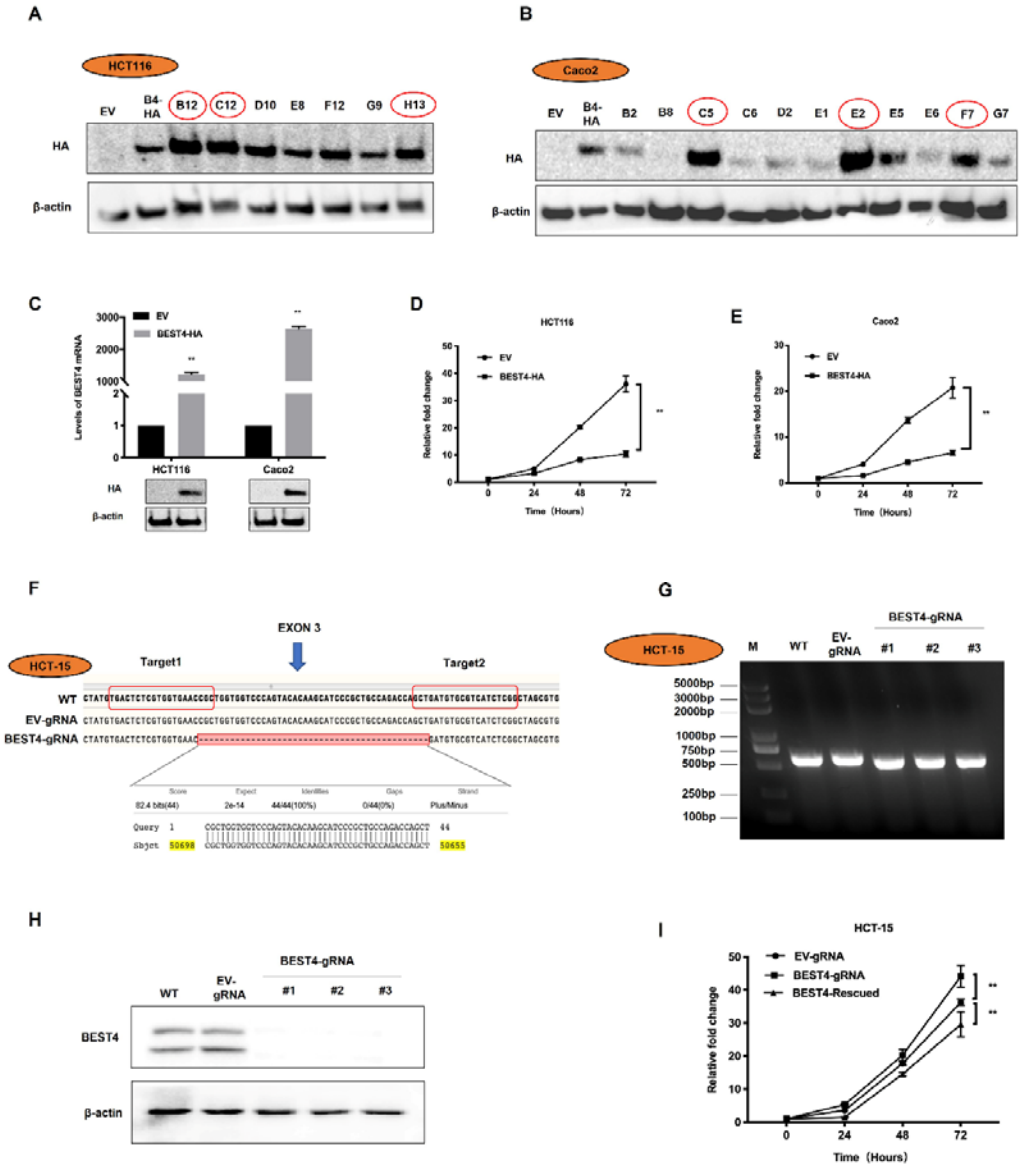

Figure 2-supplemental figure 1.

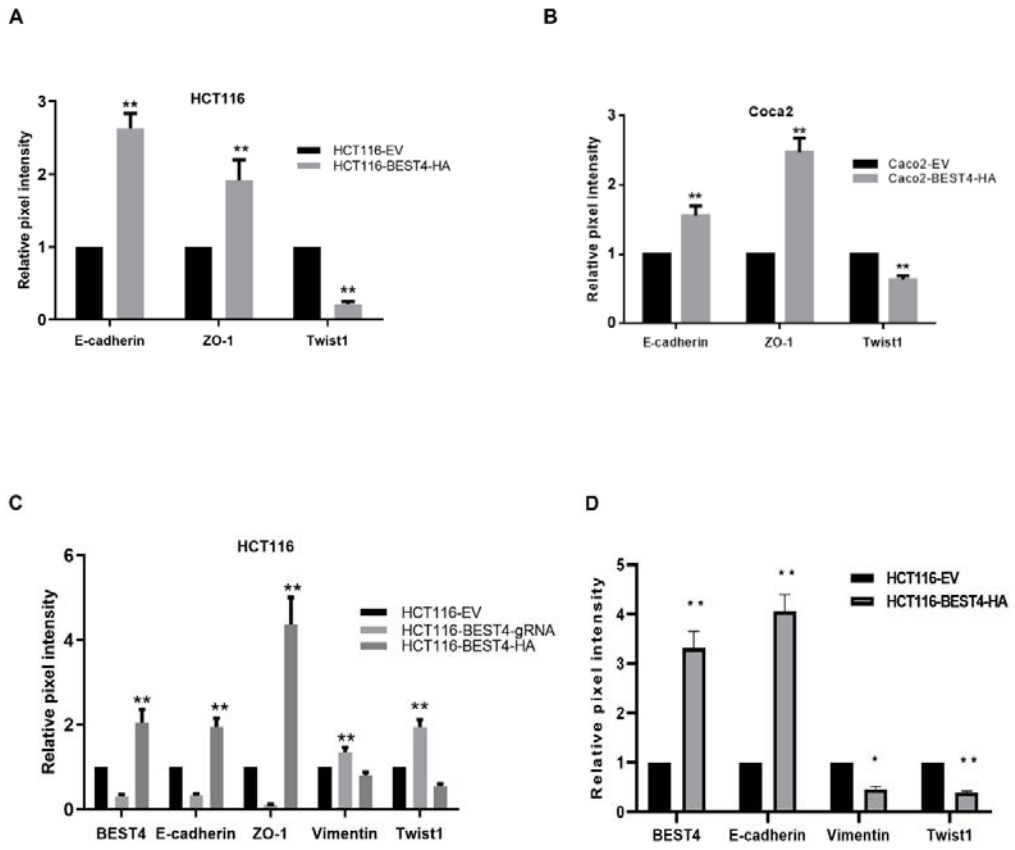

Figure 3-supplemental figure 1.

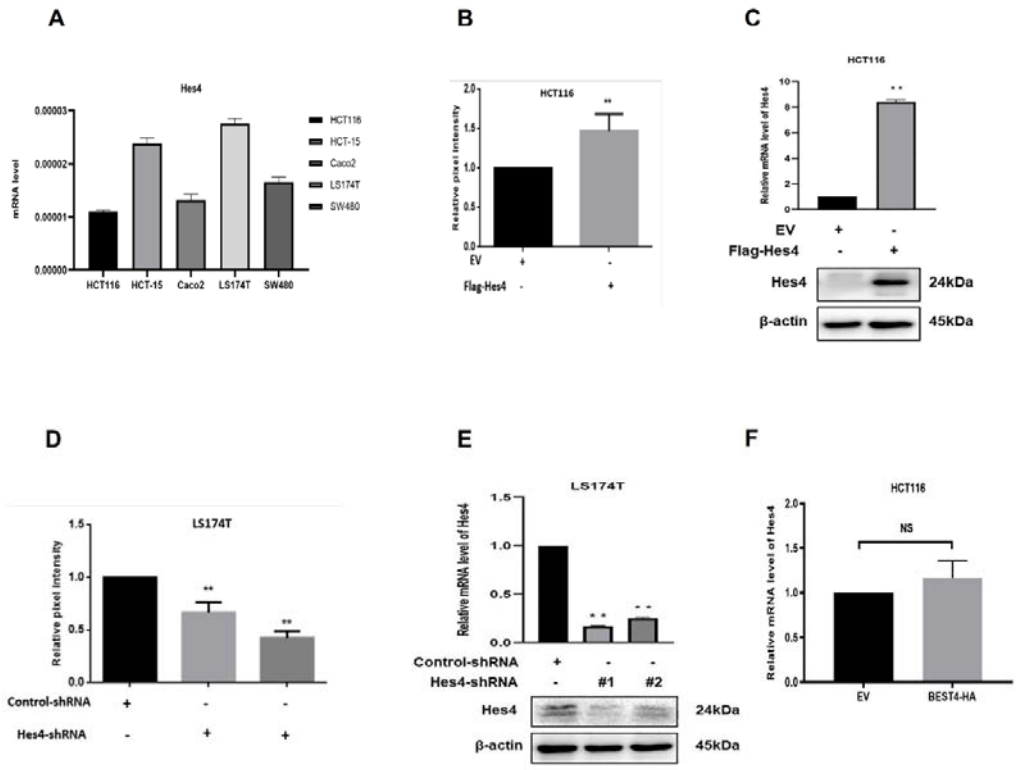

Figure 4-supplemental figure 1.

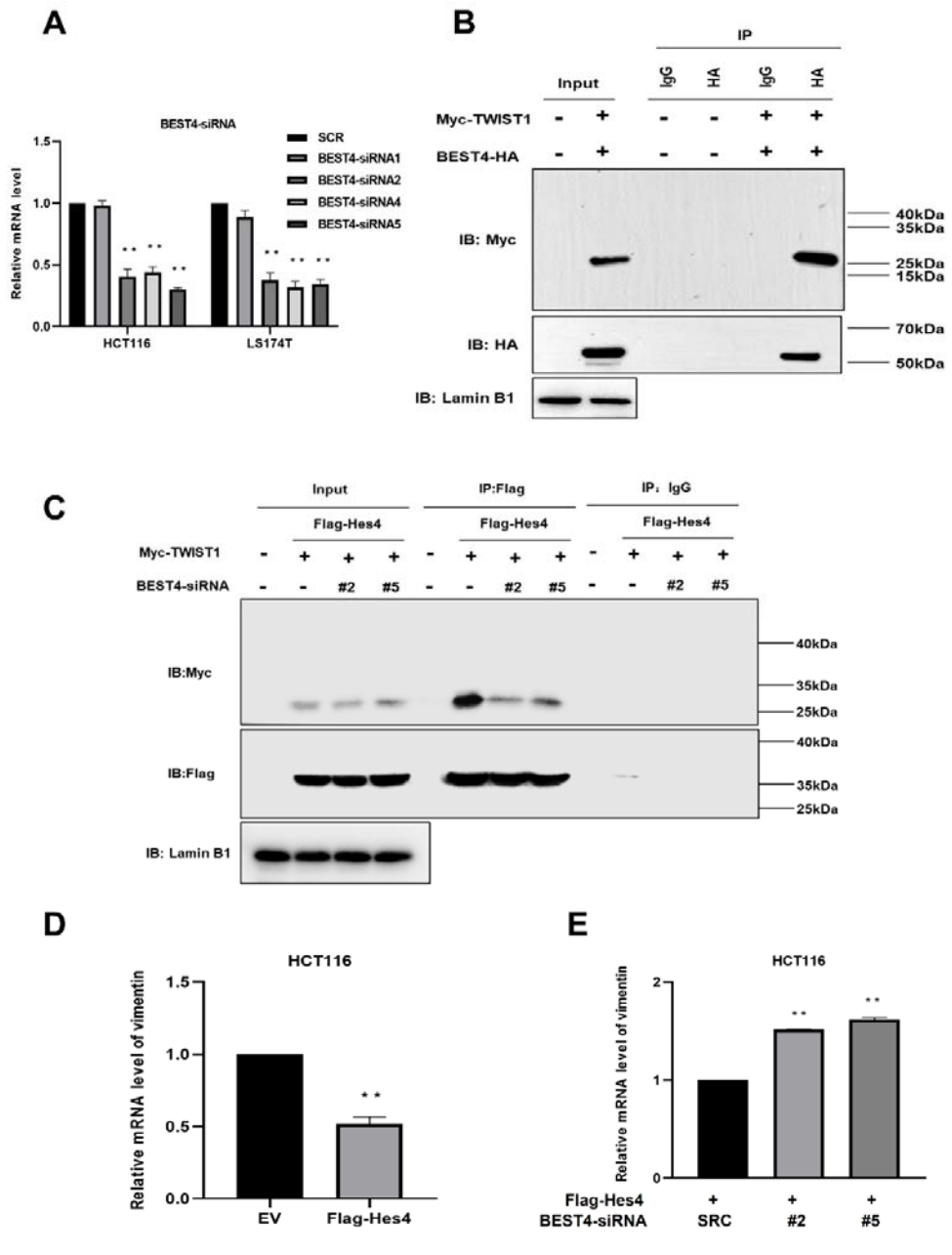

Figure 4-supplemental figure 2.

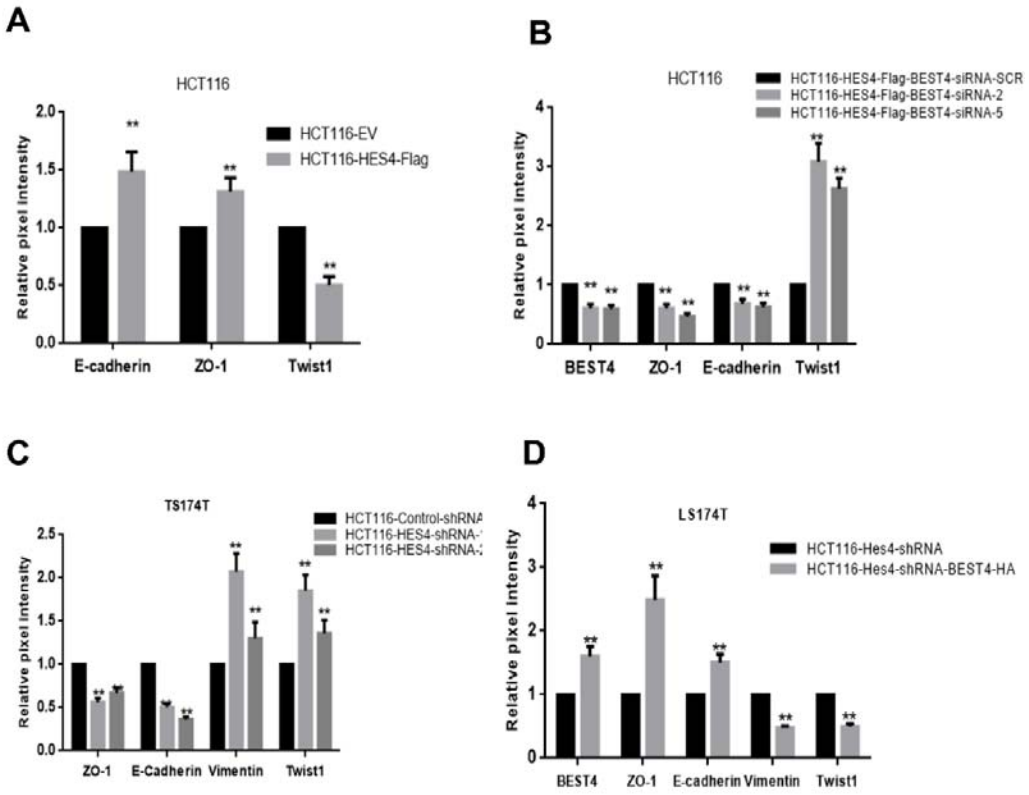

Figure 5-supplemental figure 1

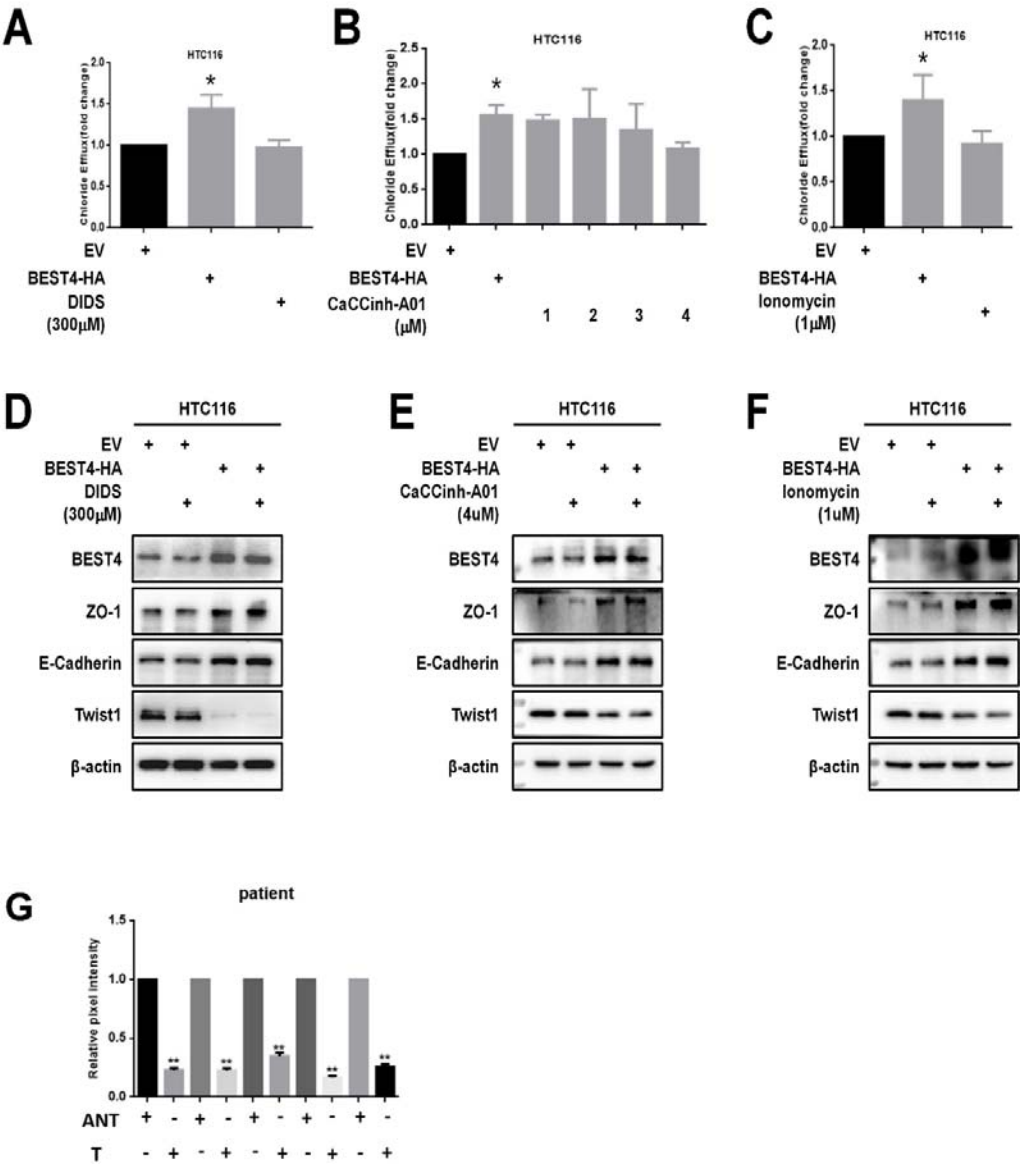

Figure 6-supplemental figure 1.

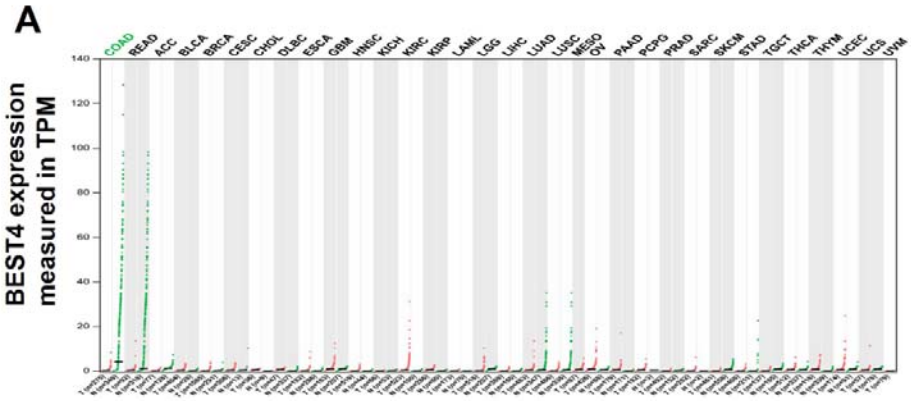

B

Gene Name	bioType	Locus	log2FC	p value
HES4	protein coding	chr1:998970-999981	-4.49	5.54E-03

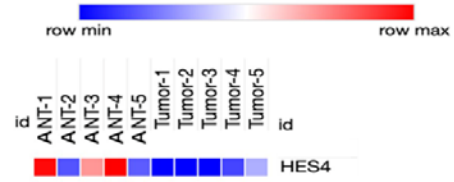

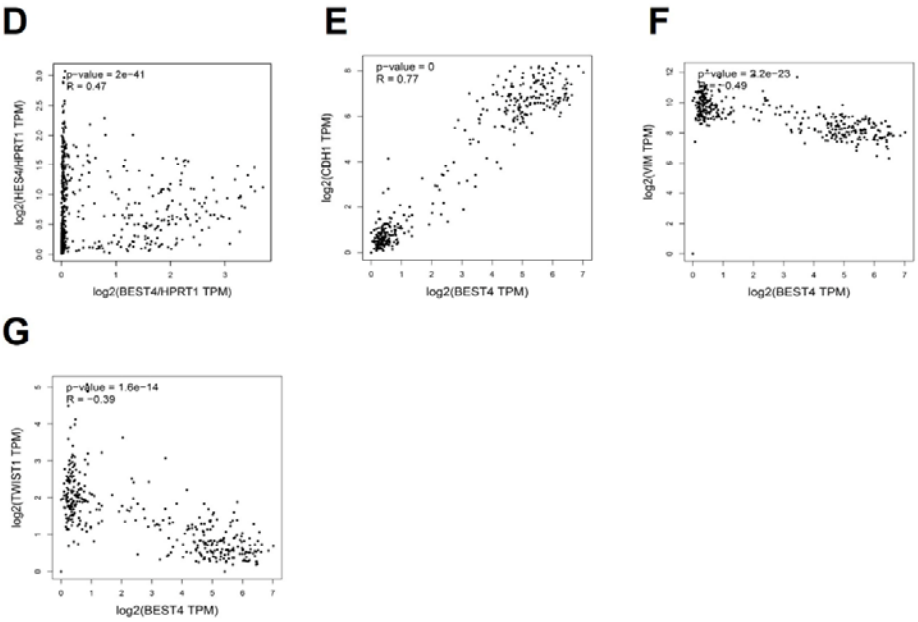

966

967

968

Table S1. The target sequence of shRNAs, siRNAs and primers used in this study.

NAME	5'-3' sequence
Hes4-shRNA 01	5'-CCACGAGTGTCTGGCGGAGGT-3'
Hes4-shRNA 02	5'-ACATCCTGGAGATGACCGTGA-3'
BEST4-siRNA 01	5'-CAAGTGCAGCATGCATTCCA-3'
BEST4-siRNA 02	5'-ATCACGGAAGGTCTTGTCAAA-3'
BEST4-siRNA 04	5'-TACCCTGGTAACCTTACTCAA-3'
BEST4-siRNA 05	5'-ACGGGCGAATACGTGACGATA-3
BEST4	Forward: 5'-CATCACCTACCGGCTG CT-3' Reverse: 5'-GCTGATGTGCGTCATCTCGG-3'
CDH1	Forward: 5'-CATCACCTACCGGCTG CT-3' Reverse: 5'-GCTGATGTGCGTCATCTCGG-3'
Vimentin	Forward: 5'-AACTTCTCAGCATCCGATGAC-3' Reverse: 5'-TTGTAGGAGTGTCGGTTGTTAAG-3'
Zo-1	Forward: 5'-AGGGGCAGTGGTGGTTTTCTGTTCTTTC-3' Reverse: 5'-GCAGAGGTCAAAGTTCAAGGCTCAAGAGG-3'
Twist1	Forward: 5'-AGCTACGCCTTCTCGGTCT-3' Reverse: 5'-CCTTCTCTGGAAACAATGACATC-3'

Hes4	Forward: 5’-GACCCGCAGTCCTCCAA-3’ Reverse: 5’-TCCGCCTTCTCCAGCTTC-3’
GAPDH	Forward: 5’-ACTCCTCCACCTTTGACGC-3’ Reverse: 5’-GCTGTAGCCAAATTCGTTGTC-3’
P1	Forward: 5’- CTCTCTGTGGCCCAGGCTGGA-3’ Reverse: 5’-GCACCAGCTGTAGTCCCAGCT-3’
P2	Forward: 5’-GAGAGGAGTCTCACTCTTT-3’ Reverse: 5’-AATGGCGTGAACCTGGGAGG-3’
P3	Forward: 5’-GCCTCCTGAGTAGCTGGGAC-3’ Reverse: 5’-TCATGAGGTCAGGAGATCGA-3’
P4	Forward: 5’-GTGATCCCACCTCTGGGCTC -3’ Reverse: 5’-CCCTGGCGTGACCTGTCGGT-3’
DHFR 5’ UTR	Forward: 5’-CTGATGTCCAGGAGGAGAAAGG-3’ Reverse: 5’-AGCCCGACAATGTCAAGGACTG-3’

971